

1 **High frequency, continuous measurements reveal strong diel and seasonal cycling of**
2 **$p\text{CO}_2$ and CO_2 flux in a mesohaline reach of the Chesapeake Bay**

3
4
5 **A. Whitman Miller^{1*}, Jim R. Muirhead¹, Amanda C. Reynolds¹, Mark S. Minton¹ and Karl**
6 **J. Klug¹**

7 ¹Smithsonian Environmental Research Center, Edgewater, MD USA

8
9 Corresponding author: A. Whitman Miller (millerw@si.edu)

10 †Additional author notes should be indicated with symbols (current addresses, for example).

11 **Key Points:**

- 12 • Automated $p\text{CO}_2$ measurements capture daily cycles and anomalous events in estuaries
13 where $p\text{CO}_2$ changes rapidly and across a wide range.
- 14 • Rhode River is net autotrophic (Dec-May), net heterotrophic (Jun-Nov), NEP is near
15 balanced annually, but can reverse status during a single day.
- 16 • Year-round continuous measurements reveal that $p\text{CO}_2$ and CO_2 flux are mediated by
17 temperature effects on biological activity and are inverse to the physical solubility of
18 CO_2 .
- 19
20

Deleted: JGR

21 ABSTRACT

22 We estimated hourly air-water gas transfer velocities (k_{600}) for carbon dioxide in the Rhode
23 River, a mesohaline subestuary of the Chesapeake Bay. Gas transfer velocities were calculated
24 from estuary-specific parameterizations developed explicitly for shallow, microtidal estuaries in
25 the Mid-Atlantic region of the United States, using standardized wind speed measurements.
26 Combining the gas transfer velocity with continuous measurements of $p\text{CO}_2$ in the water and in
27 the overlying atmosphere, we determined the direction and magnitude of CO_2 flux at hourly
28 intervals across a 3-yr record (01 July 2018 to 01 July 2021). Continuous year-round
29 measurements enabled us to document strong seasonal cycling whereby the Rhode River is
30 **primarily** autotrophic during cold-water months (Dec–May), and largely net heterotrophic in
31 warm-water months (Jun–Nov). Although there is inter-annual variability in CO_2 flux in the
32 Rhode River, the annual mean condition is near carbon neutral. Measurement at high temporal
33 resolution across multiple years revealed that CO_2 flux and **apparent** trophic status can reverse
34 during a single 24-hr period. $p\text{CO}_2$ and CO_2 flux are mediated by temperature effects on
35 biological activity and are inverse to temperature-dependent physical solubility of CO_2 in water.
36 Biological/biogeochemical carbon fixation and mineralization are rapid and extensive, so
37 sufficient sampling frequency is crucial to capture unbiased extremes and central tendencies of
38 these estuarine ecosystems.

Deleted: -

Deleted: net

Deleted: -

40 1. Introduction

41 Understanding the air-sea exchange of gases and establishing methodologies for accurate
42 measurements has been a decades-long focus of atmospheric scientists, oceanographers, and
43 biogeochemists seeking to understand interactions between oceans and the atmosphere and how
44 these interactions contribute to the global carbon cycle (Broecker et al., 1979; Wanninkhof,
45 1992, 2013). Coastal oceans and estuaries are ecosystems of interest for understanding the
46 complex nature and contribution of the land-sea interface to lateral mass transport of carbon
47 (Abril & Borges, 2005; Cai & Wang, 1998; Frankignoulle et al., 1998; Song et al., 2023) but also
48 with respect to the role these ecosystems play as both atmospheric CO_2 sources and sinks (Abril
49 & Borges, 2005; Chen et al., 2020; Dai et al., 2022; Jiang et al., 2008). The exchange of carbon
50 dioxide, methane, and other greenhouse gases (**GHGs**) between Earth's atmosphere and inland
51 waters, estuaries, coastal oceans are well-documented but not fully quantified (Abril & Borges,

Deleted: -

Deleted: -

Deleted: necessarily

Deleted: JGR

58 2005; Cai, 2011; Laruelle et al., 2017; Raymond & Cole, 2001; Raymond et al., 2013; Van Dam
 59 et al., 2019). CO₂ evasion from estuaries alone has been estimated at 15–17% of the total CO₂
 60 input from oceans to the atmosphere (Chen et al., 2020; Laruelle et al., 2017), indicating the
 61 regional and global significance of estuaries (Bauer et al., 2013; Frankignoulle et al., 1998; Jiang
 62 et al., 2008). Yet, there is still great uncertainty surrounding the true net contributions of coastal
 63 oceans, estuaries, and inland water bodies to the atmospheric loading of GHGs (Borges, 2005;
 64 Chen et al., 2020; Herrmann et al., 2020; Joesoef et al., 2015; Laruelle et al., 2017; Raymond et
 65 al., 2013; Van Dam et al., 2019).

Deleted: greenhouse gases

66
 67 To better understand the effects of estuaries on atmospheric GHG exchange and accumulation, it
 68 is imperative that we understand their capacity and function as carbon sources and sinks and
 69 ultimately how estuaries factor into the planet's overall global carbon budget (Herrmann et al.,
 70 2020; Laruelle et al., 2017; Van Dam et al., 2019). Many attempts to characterize CO₂ flux in
 71 estuaries and nearshore oceans (Chen et al., 2013; Herrmann et al., 2020; Rosentreter et al. 2021)
 72 have relied on direct measurements using floating domes, tracer gases, or, more recently, eddy
 73 covariance methods (Laruelle et al., 2017; Van Dam et al., 2019). Because flux measurements are
 74 time intensive, they tend to be temporally and spatially limited (Herrmann et al., 2020; Klaus &
 75 Vachon, 2020). Using direct flux measurements to derive accurate gas transfer velocity
 76 constants (K_o , the velocity of gas crossing the air-water boundary) enables models to be
 77 parameterized to estimate K_o and compute gas flux. Thus, correlative models that incorporate
 78 simultaneous environmental measurements such as wind and/or water velocity, factors that affect
 79 turbulence at the air-water interface and promote gas exchange, have aided in the widespread
 80 accumulation of gas flux estimates (Raymond & Cole, 2001; Van Dam et al., 2019; Wanninkhof,
 81 2014). Gas transfer velocity constant models vary according to the habitat/system being observed
 82 and chemical, physical, and biological factors present in each (e.g., lakes, rivers/streams,
 83 estuaries, and oceans; Herrmann et al., 2020; Ho et al., 2016; Raymond & Cole, 2001; Van Dam
 84 et al., 2019; Wanninkhof, 1992). To reduce uncertainty of computed gas fluxes, it is critical that
 85 the appropriate K_o models are matched to a targeted ecosystem.

Deleted: greenhouse gas

Deleted:),

Deleted: ,

Deleted: Leveraging

Deleted: k_o ,Deleted: k_o

Deleted: contemporaneous

Deleted: k_o ,

86
 87 Coastal oceans and estuaries are exceptionally complex, frequently characterized by their relative
 88 shallowness and how their freshwater inputs (riverine, surface, and groundwater) mix with salt

Deleted: JGR

98 water (Chen et al., 2020). High nutrient and pollutant loading, due to urbanization and
 99 eutrophication by humans, also have important effects on estuaries and coastal oceans (Freeman
 100 et al., 2019). High spatial and temporal variability are hallmarks of estuaries.

102 Here we present a 3_v year data set that combines high frequency (1_v min interval) measurements of
 103 dissolved and atmospheric CO₂ with co-located and continuous measurements of salinity, water
 104 temperature, tidal cycling, and wind velocity, recorded at the Smithsonian Environmental
 105 Research Center (SERC) dock, in the Rhode River, Maryland. To estimate hourly, daily,
 106 seasonal, and annual CO₂ flux rates, we applied a CO₂ gas velocity constant model developed by
 107 Van Dam et al. (2019) for the New River, North Carolina. This model is expressly designed for
 108 application to shallow, well-mixed, microtidal estuaries located in the Mid-Atlantic coast of the
 109 United States.

Deleted: -

Deleted: -

111 2. Methods

112 2.1 Study Location

113 The Rhode River is a tributary and subestuary of the Chesapeake Bay, a drowned river valley,
 114 coastal plain estuary (Fig. 1). The Rhode River has been studied extensively by SERC staff and
 115 colleagues for over 4 decades: nutrient chemistry (Jordan & Correll, 1991; Jordan et al., 1991),
 116 phytoplankton ecology (Gallegos et al., 2010), color dissolved organic matter distribution
 117 (Tzortziou et al., 2008; Tzortziou et al., 2011), and more recently, modeling of dissolved organic
 118 carbon (DOC) input from freshwater and tidal marsh sources (Clark et al., 2020). Located on the
 119 Bay's northwestern shore (38°52'N, 76°32'W), the Rhode River is bounded at its head by Muddy
 120 Creek and at its mouth by the mainstem of the Chesapeake Bay. The Rhode River is a shallow
 121 (mean depth = 2 m, max depth = 4.1 m), mesohaline (0 to 18 ppt), well-mixed, eutrophic
 122 tributary with a length of approximately 5 km; its surface area is approximately 5 km² with a
 123 shoreline perimeter of 39 km (Breitburg et al., 2008; Clark et al., 2018). A 0.21 km² tidal marsh
 124 (Kirkpatrick Marsh) fringes the estuary at the mouth of Muddy Creek (Fig. 1). Tides are semi-
 125 diurnal with a mean amplitude of approximately 30 cm, but water height can be strongly affected
 126 by wind and weather events. Muddy Creek is the main freshwater source of the Rhode River and
 127 has a maximum flow rate of 10.42 m³ · s⁻¹ and mean flow rate 0.18 m³ · s⁻¹ (mean flow = 15,552
 128 m³ · d⁻¹; Clark et al., 2020; Clark et al., 2018; Jordan et al., 1986). The mean daily volume of

Moved down [1]: In the Rhode River, we find that CO₂ flux reverses itself daily for part of the year (June–November) yielding some days that are characterized as a net sink (net autotrophic) and others that are a net source (net heterotrophic). From Dec

Moved down [2]: diel cycling is minimal and the river is almost exclusively a net sink, autotrophic both day and night. Finally, although CO₂ flux is pronounced but variable across seasons, the net CO₂ flux of the Rhode River on an annual basis is near neutral.¶

Deleted: From December to May

Formatted: Font: +Headings CS (Times New Roman), Not Bold, Underline

Deleted: sub-estuary

Deleted: , its primary source of freshwater,

Deleted: 2m

Deleted: 1m

Deleted: 500 ha

Deleted: -ha

Deleted: JGR

149 freshwater inflow from Muddy Creek is approximately 0.5% of the mean daily tidal exchange
150 volume, based on the Rhode River's area and mean tidal amplitude. In the absence of
151 measurements of the pH or $p\text{CO}_2$ of the freshwater entering the Rhode River from Muddy Creek
152 or other lesser freshwater inputs to the estuary, we are unable to report these $p\text{CO}_2$ or pH values.
153 However, given the exceedingly small overall volume of freshwater input to the Rhode River
154 from its surrounding watershed, it is not considered a river-dominated estuary so is not expected
155 to be substantially influenced by the chemical characteristics of this input. This is not to say there
156 is no freshwater influence, only that such influences are likely quite local when mixing with far
157 larger volumes of water from the Chesapeake Bay and therefore beyond the resolution of this
158 study.

Deleted: Thus, the Rhode River is not considered a river-dominated estuary. However, Gallegos et al. (1992) observed that occasional freshets emanating from the Susquehanna River, the source of 55% of all freshwater input to the Chesapeake Bay (U.S. Geological Survey, 2023), whose mouth lies 45 nautical miles (nm) up bay from the Rhode River and can cause abrupt changes in salinity and nutrient loading in the Rhode River, resulting in predictable phytoplankton blooms.

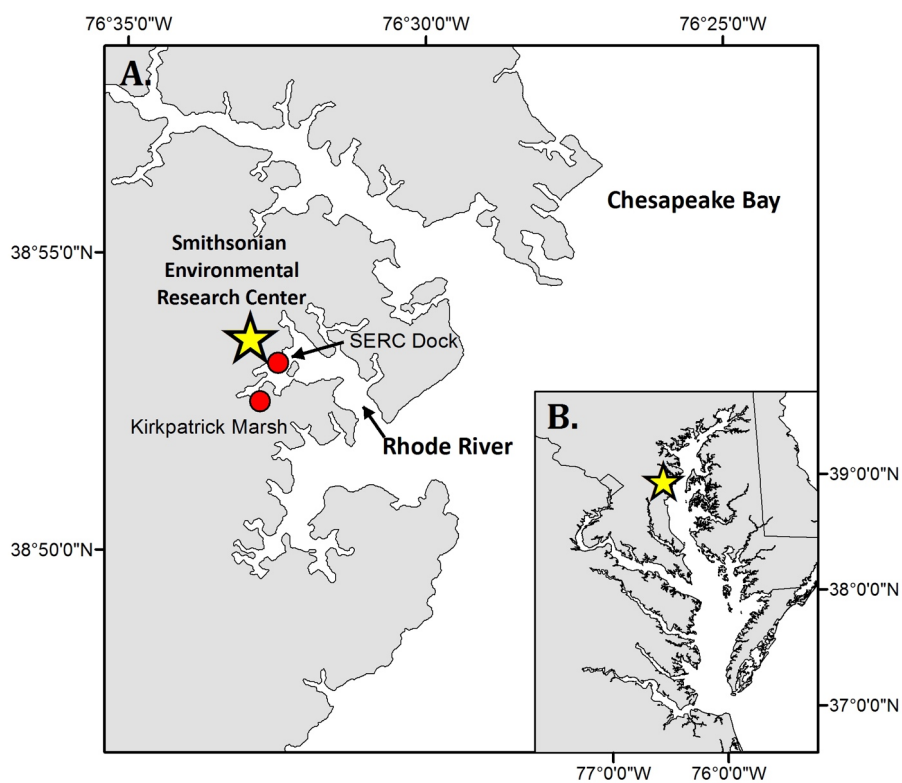
160 Although the Rhode River is a model ecosystem that has been studied intensively for several
161 decades across many dimensions (Clark et al. 2018; Correll et al., 1992; Gallegos et al., 1992;
162 Jordan et al. 1991; Rose et al. 2019), no work to date has expressly characterized the nature and
163 dynamics of CO_2 flux between the river and the atmosphere.

Deleted: with

Formatted: Font: Bold, Font color: Red

Deleted: JGR

Deleted: ¶



174 **Fig. 1.** Location of study site on the Rhode River, Edgewater MD (A), as situated in the
 175 Chesapeake Bay (B). All $p\text{CO}_2$ and related water quality values reported were measured from the
 176 SERC dock, that extends approximately 75 m from shore on Rhode River. Red circles indicate
 177 location of dock and a tidal creek that drains the Kirkpatrick saltmarsh (marsh area = 0.21 km², 1
 178 km up estuary from the dock).
 179
 180

Deleted: 75m

Deleted: ha

181 2.2 In Situ Measurements, Calculated Parameters and Quantities

182 Continuous, automated environmental measurements were made in and above the Rhode River
 183 during a 3 year period between 01 July 2018 and 01 July 2021. The purpose of these

Deleted: -

Deleted: JGR

188 measurements was to document fluctuations in aqueous $p\text{CO}_2$ on a fine time scale, from which
 189 CO_2 flux between the water and atmosphere could be calculated.

Deleted: ,

190 2.2.1 Aqueous CO_2 ($p\text{CO}_{2\text{water}}$)

191 To measure the CO_2 gradient ($\Delta C = p\text{CO}_{2\text{water}} - p\text{CO}_{2\text{air}}$) across the Rhode River surface waters
 192 and its overlying atmosphere, measurements of $p\text{CO}_2$ were made with a non-dispersive infrared
 193 (NDIR) detector. In the case of dissolved gas measurements, water was equilibrated continuously
 194 with a spherical falling film equilibrator (Miller et al. 2019). Water from 1 m below the water's
 195 surface was pumped and dispersed continuously over a 25.4 cm diameter sphere. The falling film
 196 created on the sphere generates a gas exchange surface, which forces CO_2 in the equilibrator
 197 headspace into equilibrium with the water's CO_2 content (i.e. mole fraction = $x\text{CO}_2$ ($\mu\text{mol}/\text{mol}$)).
 198 Water exits the equilibrator via an airtight drain that prevents headspace contamination from
 199 surrounding atmospheric air. Headspace gas circulates continuously in a closed loop through the
 200 equilibrator, water trap and gas dehumidifier, past the NDIR, and back into the equilibrator.
 201 Experimental observations concluded that spherical falling film equilibrators achieve 99%
 202 equilibration of CO_2 within 10–15 mins, depending on whether step changes are from low to
 203 high or high to low; details of the operation and performance of the falling film equilibrator are
 204 described in Miller et al. (2019). Measurements were made at 1 min intervals at a pressure equal
 205 to the ambient barometric pressure.

Deleted: dissolved and atmospheric

Deleted: 1m

Deleted: 4cm

Deleted: sphere's surface

Deleted: across

Deleted: CO_2

Deleted: air

Deleted: -

206
 207 Measured raw CO_2 mole fractions ($\mu\text{mol}/\text{mol}$) were converted to partial pressures (μatm) using
 208 equation 1. Minute-over-minute values were rounded down to the nearest hour and averaged to
 209 provide hourly means. The mole fractions were then evaluated with corresponding water
 210 temperature and salinity measurements following the methodology of Zeebe and Wolf-Gladrow
 211 (2001) where saturation vapor pressure of water is calculated according to Weiss and Price
 212 (1980) to determine $p\text{CO}_{2\text{water}}$.

$$214 \quad p\text{CO}_{2\text{water}} = x\text{CO}_2 \cdot (p - p\text{H}_2\text{O}) \quad (1)$$

216 where

Deleted: ,

217 $p\text{CO}_2$ = partial pressure of CO_2 of water (μatm)

218 $x\text{CO}_2$ = mole fraction of CO_2 in water ($\mu\text{mol}/\text{mol}$)

229 p = total pressure = 1 atm

230 $p_{\text{H}_2\text{O}}$ = saturation vapor pressure of water (μatm)

231

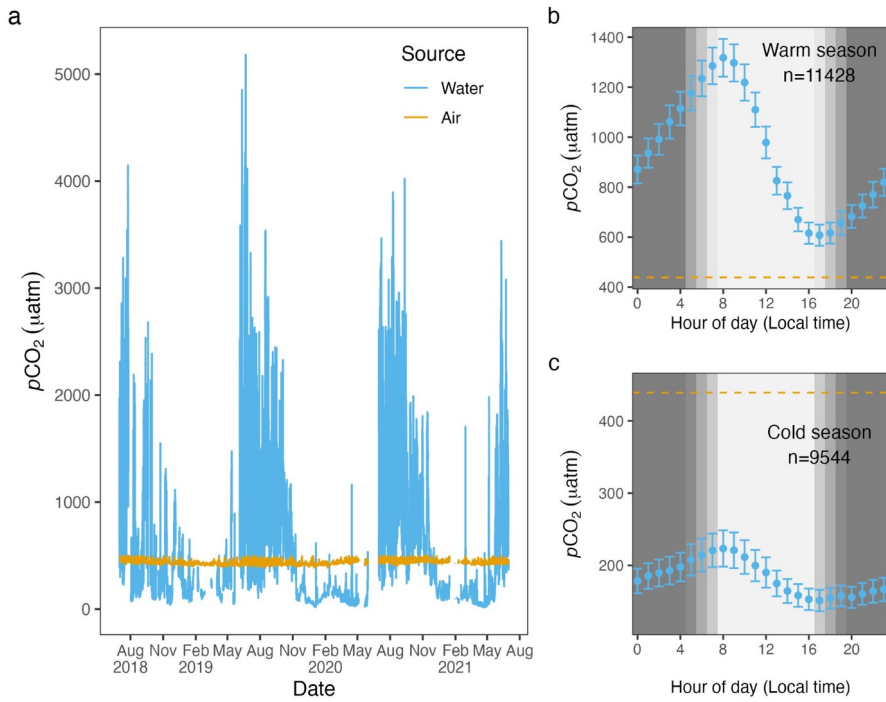
232 2.2.2 Atmospheric CO₂

233 Every six hours, the sample gas stream was automatically diverted with programmed solenoid
234 control valves from the equilibrator to an atmospheric port located approximately 5 m above the
235 pier deck. During atmospheric sampling, 15 1-min interval measurements were made. To
236 account for inaccuracies during the transition period from equilibrator to atmospheric sampling,
237 the final eight measurements were averaged and the first seven were discarded. Similarly, the
238 first 30 measurements following switchover from atmospheric port to equilibrator were
239 discarded, to ensure measurements were fully equilibrated with water. For these atmospheric
240 measurements, the contribution of the vapor pressure of water to the total atmospheric pressure
241 of the open-air environment was considered negligible (i.e. $p_{\text{H}_2\text{O}} = 0$ and $p = 1$), such that
242 $p\text{CO}_{2\text{atm}} = x\text{CO}_{2\text{atm}}$. As such, any potential differences are expected to fall well within the
243 measurement accuracy of the instrument (see below).

244

245 One advantage to using a shared NDIR sensor for aquatic and atmospheric samples is that any
246 minor effects of instrument drift will be reflected in both data streams, as opposed to two sensors
247 that drift independently of one another. Likewise, significant and sustained deviation from
248 typical local atmospheric variability will be captured during atmospheric sampling and can signal
249 the need for recalibration and assist with QA/QC of corresponding data from both streams. A
250 disadvantage of using a common sensor for both dissolved and atmospheric CO₂ measurements
251 is that it results in a mismatch in sampling frequency of the two. With this limitation in mind, we
252 chose a higher sampling frequency for aquatic measurements to better describe the inherently
253 higher variability in dissolved CO₂ in water vs. that in the atmosphere (Fig. 2).

Deleted: JGR



Deleted: 1

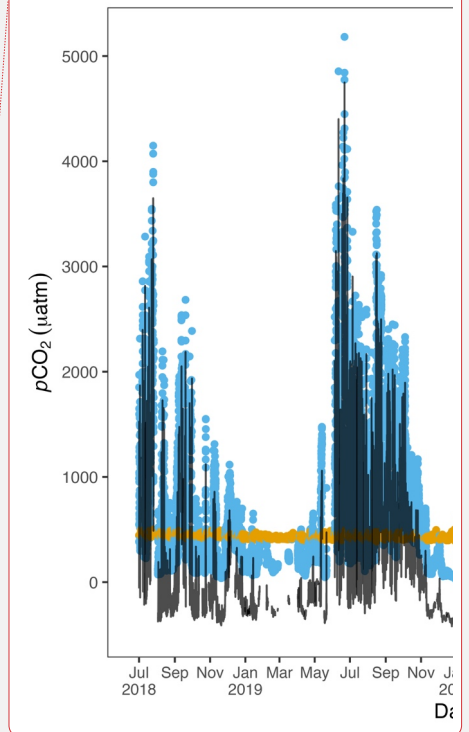


Fig. 2. Hourly $p\text{CO}_{2\text{water}}$ (blue) and $p\text{CO}_{2\text{air}}$ (goldenrod) values from 01 July 2018 to 01 July 2021 (panel a). The air-water CO_2 gradient, $\Delta C = p\text{CO}_{2\text{water}} - p\text{CO}_{2\text{air}}$, describes the directionality of gas diffusion. Negative ΔC values ($p\text{CO}_{2\text{water}}$ values falling below goldenrod demarcation) represent gas movement from air to water and vice versa. Panels b and c depict mean $p\text{CO}_{2\text{water}}$ values (95% CI) for each hour of the day for warm and cold seasons, with the dashed lines equal to the mean 3 yr value of $p\text{CO}_{2\text{air}}$.

Deleted: .

Deleted: (ΔC) is depicted with a black line, where (Δ

Deleted:).

Given the 3-yr time series and strong diel cycling of $p\text{CO}_{2\text{water}}$ (and dissolved oxygen (DO), see Figs. S1 and S2) in the Rhode River, we chose to aggregate aqueous minute-over-minute measurements to mean hourly averages. Owing to the relative lack of short-term variability in local atmospheric CO_2 concentrations (Fig. 2), we used linear interpolation to impute atmospheric CO_2 concentrations during hours in between actual readings (6-hr gaps between atmospheric measurements), which we assumed to be more realistic and reliable than Last Observation Carried Forward (LOCF) methods, where the last observation is repeated for all gaps until the next measurement is encountered, a method that has fallen out of favor, especially

Deleted: -

Deleted: ,

Deleted: measurements

Deleted: -

Deleted: JGR

280 for environmental time series data (Lachin, 2016). To determine if any inadvertent bias was
 281 introduced by linear interpolation procedure, summary statistics of actual atmospheric readings
 282 ~~and~~ actual readings + imputed CO₂ values were compared statistically. This approach enabled us
 283 to take advantage of >25,000 time points throughout the 3_{yr} period of observation, providing
 284 hourly resolution. Mean $p\text{CO}_{2\text{air}} = 437 \pm 20.0 \mu\text{atm}$ (Table 1), variability that falls well within
 285 manufacturer's specifications (see section 2.2.4).

Deleted: to

Deleted: -

287 2.2.3 CO₂ gradient (ΔC)

288 ΔC was determined by subtraction, $p\text{CO}_{2\text{water}} - p\text{CO}_{2\text{air}}$, where positive ΔC values correspond to
 289 higher CO₂ concentrations in the water, tending toward movement from water to air (outgassing
 290 ~~or evasion~~, where Rhode River = CO₂ source), and negative values that signal CO₂ ~~transport~~
 291 from air to water (dissolution, where Rhode River = CO₂ sink). Figure 2 shows $p\text{CO}_{2\text{water}}$ ~~and~~
 292 $p\text{CO}_{2\text{air}}$ plotted on an hourly basis for the 3_{yr} period beginning 01 July 2018 and ending 01 July
 293 2021. ~~Across this period, ΔC was predominantly negative during cold months and predominantly~~
 294 ~~positive during warm months when $p\text{CO}_{2\text{water}}$ tended to reach the highest values of the year, but~~
 295 ~~ΔC sometimes reversed sign due to occasional extreme day-time photosynthetic drawdown of~~
 296 ~~CO₂~~ (Fig. 2).

Deleted: movement

Deleted: transport

Deleted: Values of

Deleted: ,

Deleted: , and ΔC are

Deleted: -

298 2.2.4 Accuracy of CO₂ measurements

299 Estimated accuracy of the spherical falling film equilibrator and NDIR sensor (SenseAir K30,
 300 <https://senseair.com/>) combination were experimentally determined in the lab and found to
 301 measure water equilibrated with known gas concentrations to be within the $\pm 1\%$ uncertainty
 302 limits of the of certified standard gas mixtures used, and well within the published accuracy
 303 specification of the SenseAir K30 (i.e., $\pm 30 \text{ ppmv} \pm 3\%$ of instrument reading). Experimental
 304 analysis by Martin et al. (2017) report even higher accuracy when relative humidity and
 305 atmospheric pressure are controlled for. Details on performance of the spherical falling film
 306 equilibrator, such as accuracy, precision, and time constants can be found in Miller et al. (2019).
 307 Although SenseAir offers automated calibration via long term comparisons to atmospheric
 308 readings, this feature was deactivated. The K30 NDIR was periodically validated using standard
 309 zero CO₂ (nitrogen) and standard certified span gases at intervals of one to two months during
 310 the study period. Although the K30 was never observed to drift beyond its factory specifications,

Deleted: l

320 the sensor was occasionally re-calibrated in the lab, ~~and~~ measured values were accepted without
 321 adjustment.

322
 323 CO₂ measurements were downloaded to a database at approximately two-week intervals during
 324 the observation period. Data were graphed and reviewed visually, in combination with twice
 325 weekly observations of equilibrator function recorded in an accompanying notebook. Anomalous
 326 data were flagged and excluded from data analysis (e.g., flooding or clogging events that
 327 interrupted proper equilibration.)
 328

329 2.3 Co-located water quality and atmospheric measurements

330 This water quality station at the SERC dock is a long-term node of the Maryland Department of
 331 Natural Resources “Eyes on the Bay” Chesapeake Bay tidal water monitoring program, and has
 332 been operated by the SERC since 1986. Water quality and atmospheric data are maintained by
 333 the MarineGEO Upper Chesapeake Bay Observatory and can be accessed online (Benson et al.,
 334 2023). A YSI EXO2 sonde was positioned 1 m below the water’s surface and in proximity (~2, 5
 335 m distance) to the submerged water pump that fed the pCO₂ equilibrator. Sonde measurements
 336 were made at 6 minute intervals and aggregated to 1 hr averages. The published accuracy
 337 specifications for the YSI sonde are as follows: temperature: ±0,01 °C (-5° to 35° C); salinity:
 338 ±1% of reading or 0,1 ppt (0–70 ppt); dissolved oxygen: ±0.1 mg/L or 1% of reading (0 to 20
 339 mg/L). Discrete measurements of temperature and salinity were made with a handheld YSI
 340 Professional Plus 2030 with Quattro Cable instrument, with the following specifications:
 341 temperature: ±0,02 °C (-5° to 70° C); salinity: ±1% of reading or 0,1 ppt (0–70 ppt); dissolved
 342 oxygen: ±0.2 mg/L or 2% of reading (0 to 20 mg/L). Equilibrator temperature was measured
 343 with a probe (EDS model OW-TEMP-B3-12xA) accurate to ±0,5 °C (-10° to 85 °C). Discrete
 344 measurements were routinely compared with the sonde to corroborate measurement agreement.
 345 Wind speed measurements were made using a sonic anemometer (Vaisala WXT-520 weather
 346 transmitter) mounted 7 m above the mean low tide height of the water and located directly above
 347 the pCO₂ equilibrator.

349 2.4 Data Processing

350 Data included in this study span 01 Jul 2018 to 01 Jul 2021.

Deleted: JGR

Deleted: but

Deleted: 1m

Deleted: 5m

Deleted: -

Deleted: -

Deleted: measurements

Deleted: T

Deleted: 01°C

Deleted:); Salinity

Deleted: 1ppt (0–70

Deleted:); Dissolved

Deleted: Discrete water samples were taken approximately weekly from the equilibrator feed water to evaluate total alkalinity, ...

Deleted: temperature and

Deleted: measurements

Deleted: . Temperature

Deleted: 02°C (-5°C

Deleted: 70°C); Salinity

Deleted: 1ppt

Deleted: D

Deleted: Temperature:

Deleted: 5°C (-10

Formatted: Underline

Deleted: JGR

374 2.4.1 Gas-specific solubility

Deleted: ¶

375 To determine the purely physical effects of temperature and salinity on CO₂ solubility, gas-
 376 specific solubility values K_0 (mmol · m⁻³ · μatm⁻¹) were calculated across the 3_v yr observation
 377 period using water temperature and salinity measurements in combination with $p\text{CO}_{2\text{water}}$ values,
 378 according to Weiss and Price (1980) at 1_v hour intervals.

Deleted: -

Deleted: -hr frequencies.

380 2.4.2 Gas transfer velocity estimation (k)

381 Given the similarities between the Rhode River and New River estuaries (e.g., shallow,
 382 microtidal estuaries with slow water velocity and strong diel cycles in $p\text{CO}_2$ and DO), we chose
 383 to parameterize gas transfer velocity k (cm · h⁻¹) standardized to the unitless Schmidt number
 384 600 (k_{600}) according to the estuary-specific k parameterization model developed by Van Dam et
 385 al. (2019). Van Dam et al. (2019) determined that k correlated with wind speed differently during
 386 daytime versus nighttime hours (linear vs. parabolic relationships). Wind speed data were
 387 collected during the 3_v yr period from a sonic anemometer located on the SERC dock directly
 388 above the equilibration system and approximately 7 m above the water's surface at mean low
 389 tide height. For the analysis, windspeeds were standardized for a height of 10 m following a
 390 power-law relationship, $U_{10} = U_7 * (10/7)^{0.15}$ (Saucier, 2003). Following Van Dam et al.,
 391 wind speed data were binned to 1.5 m s⁻¹ intervals for day and night readings and raw values
 392 replaced by the mean wind speed for each bin. The median binned windspeed over the Rhode
 393 River was 2.2 m s⁻¹, regardless of time of day or season. Recorded windspeeds never exceeded
 394 10m s⁻¹ and were dominated by much lower values (Fig. S1). Unlike the New River Estuary, the
 395 Rhode River's windspeed profile does not differ much between day and night, nor across season.
 396 For this reason, we chose to use the most conservative k_{600} formulation from Van Dam et al
 397 (2019), that combines day and night winds to estimate k_{600} .

Deleted:) for shallow, microtidal estuaries.

Deleted: the day than

Deleted: -

Deleted: Wind

Deleted: /

399 Wind speed was used to parameterize k_{600} as follows:

$$401 \quad k_{600} = 1.5 * U_{10} + 4.2 \quad (2)$$

402 where U_{10} = mean of binned wind speed at 10 m above the water's surface (m · s⁻¹).

404

Deleted: JGR

413 2.4.3 CO₂ flux

414 Using continuous, parallel 3-yr records (01 July 2018 to 01 July 2021) of dissolved and
 415 atmospheric *p*CO₂, water temperature, salinity, and wind speed (at standard 10m height, *U*₁₀),
 416 CO₂ flux was derived according to the equation:

Deleted: -

417
 418
$$\text{CO}_2 \text{ flux} = k_{600} \cdot K_0 \cdot \Delta C \cdot (600 / Sc)^{-0.5} \quad (3)$$

419 where

Deleted: ,

420 CO₂ flux = the rate and direction of CO₂ mass moving between water and gas phases

421 (mmol · m⁻² · hr⁻¹)

422 *k*₆₀₀ = gas transfer velocity (cm · hr⁻¹), normalized to a common Schmidt number

423 (*Sc* = 600)

424 *K*₀ = gas-specific solubility for CO₂ (mmol · m⁻³ · μatm⁻¹)

425 Δ*C* = air-water concentration gradient (μatm)

426 *Sc* = Schmidt number

427
 428 Note: CO₂ flux calculations require conversion from traditional *k*₆₀₀ units (cm · hr⁻¹) to (m · hr⁻¹)
 429 from Δ*C* units (μatm) to (atm) prior to calculation.

431 2.4.4 Day/Night Designation

432 To differentiate daytime from nighttime hours, we used the position of the measurements
 433 (latitude) in the Rhode River, combined with the local date and time. This approach enabled us to
 434 uniformly designate various environmental measurements as happening during the day or night
 435 (R package "LakeMetabolizer", Winslow et al., 2016).

437 2.4.5 Seasonality

438 We chose to break the year into two 6-month periods based seasonal water temperature shifts,
 439 designating June–November as “warm-water months” when water temperatures averaged 23.2 ±
 440 6.90 °C. (mean ± 1 sd) and December–May as “cold-water months”, 10.9 ± 5.66 °C (Figs. S1 and
 441 S2).

Deleted: -mo

Deleted: in the spring and fall

Formatted: Font color: Text 1

Formatted: Font color: Text 1

Formatted: Font color: Text 1

Deleted: and Dec

Deleted: " (Fig. S1).

Formatted: Font color: Text 1

Formatted: Underline

Deleted: JGR

450 2.4.6 Effect size

451 Owing to the large number of observations available for comparison in this study, the likelihood
 452 of finding statistically significant results is quite high. Whether such statistical results by
 453 themselves connote practical and informative differences can be difficult to discern. Effect sizes
 454 (Omega-squared, ω^2) were calculated according to two-factor ANOVAs where independent
 455 variables were investigated by season (cold-water vs. warm-water season), day/night period and
 456 the interaction of season and day/night. The independent variables compared were: K_0 , CO_2 flux,
 457 $\Delta p\text{CO}_2$, k_{600} , $p\text{CO}_{2\text{air}}$, $p\text{CO}_{2\text{water}}$, and wind speed. To account for temporal autocorrelation and
 458 lack of independence of observations that are typical of environmental time series data, we
 459 corrected for overinflation in the residual mean square used in the effect size calculations by
 460 removing the autocorrelation present within residuals, leaving the white-noise component as the
 461 unbiased estimate of residual variability (Cochrane-Orcutt procedure, R package "orcutt", Spada
 462 et al., 2018).

Deleted: So, effect

463

464 **3. Results and Discussion**

465 3.1 Daily and Seasonal Cycling of $p\text{CO}_2$

466 Hourly averaged measurements of $p\text{CO}_{2\text{water}}$ in the Rhode River across three years revealed
 467 strong diel and seasonal cycling (Fig. 2). Mean and maximum $p\text{CO}_{2\text{water}}$ were significantly higher
 468 in warm-water vs. cold-water months (Table 1). During warm-water months (Jun–Nov) daily
 469 oscillations of $p\text{CO}_2$ frequently transit from far above to below ambient atmospheric conditions
 470 over the course of the day, only to reverse direction (from low to high) during the nighttime
 471 hours (Fig. 2). During the summer, $p\text{CO}_{2\text{water}}$ levels sometimes shifted by as much as 4500 μatm
 472 in both directions during a single 24 hr period (Fig. 2). This pattern is consistent with
 473 biologically driven cycling whereby very high early morning $p\text{CO}_{2\text{water}}$ conditions are depleted
 474 by net photosynthetic activity (inorganic carbon fixation) over the course of the day, but high
 475 $p\text{CO}_{2\text{water}}$ is restored by respiration in the benthos and water column at night (Song et al. 2023).
 476 Comparing dissolved oxygen (DO) over the same period, similar harmonic cycling is observed,
 477 but maximums and minimums of $p\text{CO}_2$ and DO were inversely related (Fig. S1), hallmarks of a
 478 production/respiration driven system (Herrmann et al., 2020; Van Dam et al., 2019).

Deleted: e

Deleted: 3

Deleted: -

Deleted: 3

479

Deleted:Page Break.....

486 Table 1. Descriptive statistics comparing seasonality of pCO₂, CO₂ flux and associated
 487 parameters in cold-water (Dec–May) and warm-water seasons (Jun–Nov).
 488

Season	Time Period	Variable	Units	N	Mean	Min	Max	SD
overall	l	CO ₂ flux	mmol · m ⁻² · hr ⁻¹	2097	-0.09	-4.89	11.18	1.823
cold	day	CO ₂ flux	mmol · m ⁻² · hr ⁻¹	4494	-1.39	-4.89	8.26	1.134
cold	night	CO ₂ flux	mmol · m ⁻² · hr ⁻¹	5050	-1.39	-4.66	5.24	0.927
warm	day	CO ₂ flux	mmol · m ⁻² · hr ⁻¹	6007	1.18	-3.95	11.18	1.731
warm	night	CO ₂ flux	mmol · m ⁻² · hr ⁻¹	5421	0.78	-3.97	8.05	1.467
overall	l	K ₀	mmol · m ⁻³ · matm ⁻¹	2097	0.04	0.03	0.07	0.011
cold	day	K ₀	mmol · m ⁻³ · matm ⁻¹	4494	0.05	0.03	0.07	0.009
cold	night	K ₀	mmol · m ⁻³ · matm ⁻¹	5050	0.05	0.03	0.07	0.008
warm	day	K ₀	mmol · m ⁻³ · matm ⁻¹	6007	0.03	0.03	0.06	0.007
warm	night	K ₀	mmol · m ⁻³ · matm ⁻¹	5421	0.04	0.03	0.07	0.008
overall	l	k ₆₀₀	cm · hr ⁻¹	2097	7.86	5.57	18.36	2.047
cold	day	k ₆₀₀	cm · hr ⁻¹	4494	8.71	5.57	16.33	2.251
cold	night	k ₆₀₀	cm · hr ⁻¹	5050	7.74	5.57	18.36	2.081
warm	day	k ₆₀₀	cm · hr ⁻¹	6007	7.92	5.57	18.36	1.868
warm	night	k ₆₀₀	cm · hr ⁻¹	5421	7.20	5.57	18.36	1.751
overall	l	DC	matm	2097	154	-436	4750	645.8
cold	day	DC	matm	4494	-239	-436	1553	220.9
cold	night	DC	matm	5050	-256	-434	1204	164.2
warm	day	DC	matm	6007	570	-399	4750	745.5
overall	l	pCO _{2air}	matm	2097	437	387	500	20.0
cold	day	pCO _{2air}	matm	4494	430	390	497	16.0

Deleted: JGR

Formatted ... [1]

Formatted ... [3]

Formatted ... [2]

Deleted: e

Formatted ... [4]

Formatted ... [5]

Formatted ... [7]

Formatted ... [6]

Formatted ... [8]

Formatted ... [9]

Formatted ... [10]

Formatted ... [11]

Formatted ... [12]

Formatted ... [13]

Formatted ... [14]

Formatted ... [15]

Formatted ... [20]

Formatted ... [21]

Formatted ... [16]

Formatted ... [22]

Formatted ... [18]

Formatted ... [19]

Formatted ... [24]

Deleted: 1

Deleted: 885

Deleted: 177

Formatted ... [25]

Formatted ... [26]

Formatted ... [27]

Formatted ... [28]

Formatted ... [29]

Formatted ... [30]

Formatted ... [17]

Formatted ... [23]

Formatted ... [36]

Formatted ... [37]

Formatted ... [38]

Deleted: 0

Deleted: 885

Deleted: 4

Deleted:

Formatted ... [31]

Formatted ... [33]

Formatted ... [34]

Formatted ... [35]

Formatted ... [40]

Formatted ... [41]

Formatted ... [42]

Formatted ... [43]

Formatted ... [44]

Formatted ... [45]

Formatted ... [32]

Formatted ... [46]

Formatted ... [47]

Formatted ... [39]

Formatted ... [53]

Formatted ... [54]

Formatted ... [55]

Deleted: 388

cold	night	pCO _{2air}	matm	5050	432	387	499	17.8
warm	day	pCO _{2air}	matm	6007	439	390	499	20.7
warm	night	pCO _{2air}	matm	5421	443	387	500	21.5
overall		pCO _{2water}	matm	2097	591	15	5182	651.8
cold	day	pCO _{2water}	matm	4494	191	15	1982	220.9
cold	night	pCO _{2water}	matm	5050	176	17	1638	163.9
warm	day	pCO _{2water}	matm	6007	1009	47	5182	752.6
warm	night	pCO _{2water}	matm	5421	844	38	4855	632.2
overall		wind	m · s ⁻¹	2097	2.4	0.1	9.8	1.42
cold	day	wind	m · s ⁻¹	4494	3.1	0.3	8.9	1.53
cold	night	wind	m · s ⁻¹	5050	2.4	0.3	9.1	1.45
warm	day	wind	m · s ⁻¹	6007	2.5	0.1	9.8	1.28
warm	night	wind	m · s ⁻¹	5421	2.0	0.1	9.1	1.23

633
 634 On the seasonal timescale, pCO₂ was consistently lowest and DO highest during cold-water
 635 months of the year (Dec–May; Fig. S1). Importantly, for both gases the temporal variability (diel
 636 cycling; Fig. S2) was most constrained during cold-water months across years, strongly
 637 suggesting that carbon fixation exceeds respiration for prolonged periods (weeks to months). In
 638 contrast, during warm-water months (Jun–Nov), photosynthesis/carbon fixation and respiration
 639 are more evenly balanced, compensating one another over 24 hr periods (i.e., respiration >
 640 productivity at night and productivity > respiration during daylight hours; Fig. 2).

642 3.2 Air-water concentration gradient = ΔC (μatm)

643 When hourly pCO_{2water} and pCO_{2air} values (composed of 4 hourly measurements and 20
 644 interpolated values per day) were plotted across the three years of observation, the diel and
 645 seasonal cycles of pCO_{2water} are evident. As expected, atmospheric concentrations of CO₂
 646 remained relatively constant compared with aqueous loads. When the mean raw pCO_{2air}
 647 measurements (mean = 435.1, 95% CI [434.4, 435.7]) were compared with raw pCO_{2air}

Deleted: JGR
 Formatted ... [354]
 Formatted ... [355]
 Deleted: .078
 Deleted: .000
 Deleted: 498.556
 Deleted: 807
 Formatted ... [348]
 Formatted ... [350]
 Formatted ... [351]
 Formatted ... [352]
 Formatted ... [353]
 Formatted ... [357]
 Formatted ... [358]
 Formatted ... [359]
 Formatted ... [360]
 Formatted ... [361]
 Formatted ... [362]
 Formatted ... [363]
 Formatted ... [349]
 Formatted ... [356]
 Formatted ... [370]
 Formatted ... [371]
 Formatted ... [364]
 Formatted ... [366]
 Formatted ... [367]
 Formatted ... [368]
 Formatted ... [369]
 Formatted ... [373]
 Formatted ... [365]
 Deleted: .103
 Deleted: 389.648
 Deleted: .444
 Deleted: 668
 Formatted ... [374]
 Formatted ... [375]
 Formatted ... [376]
 Formatted ... [377]
 Formatted ... [378]
 Formatted ... [379]
 Formatted ... [372]
 Formatted ... [386]
 Formatted ... [387]
 Deleted: .326
 Deleted: 386.667
 Deleted: 499.889
 Deleted: 459
 Formatted ... [380]
 Formatted ... [382]
 Formatted ... [383]
 Formatted ... [384]
 Formatted ... [381]
 Formatted ... [385]
 Formatted ... [389]
 Formatted ... [390]
 Formatted ... [391]
 Formatted ... [392]
 Formatted ... [393]
 Formatted ... [394]
 Formatted ... [388]

Deleted: JGR

764 measurements + imputed estimates (mean = 435.4, 95% CI [435.2, 435.7]) no statistical
765 difference was observed, indicating that no substantial bias was introduced by linear
766 interpolation of atmospheric measurements.

767

768 Although nearshore atmospheric CO₂ concentrations are expected to vary more than those in
769 isolated well-mixed atmosphere (e.g., [at the](#) Mona Loa Observatory), annual mean values were
770 consistent and within the published uncertainty of the K30 NDIR sensor, when compared with
771 global measurements conducted at Mona Loa ([Thoning et al., 2023](#)). ~~Local~~ perturbations (e.g.,
772 effects of terrestrial photosynthetic drawdown when wind is absent) ~~were apparent in~~
773 ~~measurements (Fig. 2) but~~ there were no instances when the measured local atmospheric values
774 were suspiciously high or low for days on end, as compared with expected global mean
775 atmospheric values for the time period (i.e., 408–416 ppmv; <https://www.co2.earth/annual-co2>,
776 [Thoning et al., 2023](#)). This lack of sustained anomalous deviation served as additional
777 confirmation that the K30 was functioning properly and had not drifted outside its calibration
778 range. Importantly, given the extreme diel cycling and seasonal variability of the Rhode River's
779 *p*CO_{2water}, the absolute accuracy necessary for determining year-over-year changes in
780 atmospheric or ocean *p*CO₂ is not a requirement for these CO₂ flux calculations which rely on
781 relative differences between water and atmospheric measurements.

Deleted: Variability at the 6-hr measurement scale was shown to be considerable, reflecting expected local

Deleted:), yet

782

783 Hourly air-water concentration gradient values = ΔC (μatm) were calculated and plotted across
784 the three years of study (Fig. 2). During warm months, *p*CO_{2water} routinely shifts from
785 supersaturated to sub-atmospheric and back again, over the course of 24 hours (e.g., between
786 >2000 μatm and <410 μatm on a single day). These large daily swings in *p*CO_{2water} produced
787 concomitant directional reversals of ΔC ($p\text{CO}_{2\text{water}} - p\text{CO}_{2\text{air}}$), which result in longer term
788 averaged gradients (e.g., multi-day, multi-week averages) near zero (Fig. 2). In contrast, ~~most of~~
789 ~~the~~ time during cold-water months is spent in a state of sub-atmospheric *p*CO_{2water} (under-
790 saturation with respect to overlying atmosphere), resulting in ΔC values that are negative and
791 which promote movement of CO₂ from the atmosphere into the water.

Deleted: consistent,

Formatted: Font: +Headings CS (Times New Roman)

Deleted: majority

Deleted: over prolonged periods

792

793 3.3 Gas-specific solubility (*K₀*)

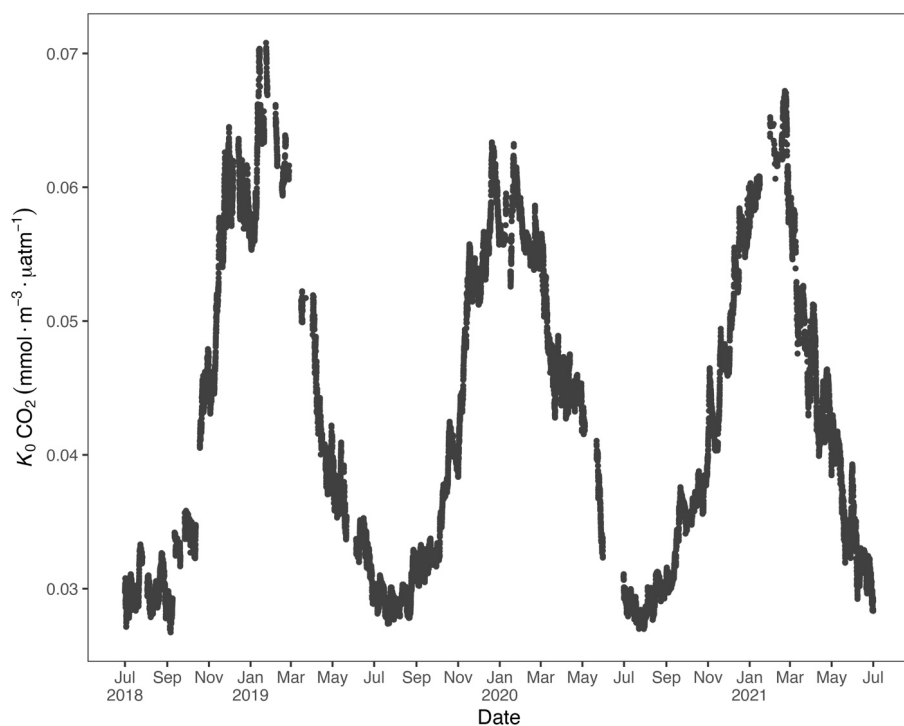
Deleted: JGR

800 To account for the physical effects of temperature and salinity on the solubility of CO₂ in
 801 estuarine water, K_0 was calculated by methods of Weiss and Price (1980). K_0 varied strongly
 802 across seasons over the 3 yr observation period. The maximum annual range = 0.027 to 0.071
 803 mmol · m⁻³ · μatm⁻¹; mean cold-water months = 0.051 and mean warm-water months = 0.035
 804 mmol · m⁻³ · μatm⁻¹, confirming that CO₂ was most soluble during winter and least soluble in
 805 summer (Fig. 3). This is inverse to observed dissolved CO₂ values: $p\text{CO}_{2\text{water}}$ was lowest and
 806 least variable during winter and highest and most variable during summer (Fig. 2, Table 1)
 807 suggesting that solubility, in and of itself, plays only a minor and non-limiting role in $p\text{CO}_{2\text{water}}$
 808 in the Rhode River. Effect size (ω^2) estimates indicated that the greatest proportion of variability
 809 in K_0 was associated with season, vs. day/night or the interaction of the two (Table 2).

Deleted: the

Deleted: -

Deleted: 4



Deleted: 4

810
 811 **Fig. 3.** Gas-specific solubility (K_0) for CO₂ based on water temperature and salinity.
 812 Units are mmol m⁻³ μatm⁻¹ in the Rhode River (01 Jul 2018 to 01 Jul 2021).

Deleted: 4

Deleted:)

Deleted: JGR

819 **Table 2.** Contrast effect sizes based on two-factor ANOVA where independent variables were
 820 compared by season (cold-water season = Dec–May vs warm-water season = Jun–Nov),
 821 day/night period and the interaction of the two. ω^2 is a measure of effect size, estimating the
 822 proportion of total variance explained by each parameter. Effect sizes were corrected for inherent
 823 temporal autocorrelation using the Cochrane-Orcutt procedure (Spada et al., 2018).
 824

Deleted: –

Deleted: e

Deleted:

Variable	Factor	Effect Size (ω^2)
K_0	Season	0.0300
K_0	Day/Night	0.000575
K_0	Season:Day/Night	0.0000140
CO ₂ flux	Season	0.415
CO ₂ flux	Day/Night	0.00295
CO ₂ flux	Season:Day/Night	0.00301
ΔC	Season	0.310
ΔC	Day/Night	0.00501
ΔC	Season:Day/Night	0.00333
k_{600}	Season	0.00164
k_{600}	Day/Night	0.00269
k_{600}	Season:Day/Night	0.0000549
pCO_{2air}	Season	0.000137
pCO_{2air}	Day/Night	0.0000134
pCO_{2air}	Season:Day/Night	0.00000137
pCO_{2water}	Season	0.188
pCO_{2water}	Day/Night	0.00275
pCO_{2water}	Season:Day/Night	0.00191
wind speed	Season	0.00711
wind speed	Day/Night	0.0186
wind speed	Season:Day/Night	0.000182

Deleted: ¶

Deleted: ¶

Deleted:

Deleted: ¶

825

826 3.4 Temperature/Biology ratio

827 To independently parse the magnitude of the physical versus biological forcing of pCO_{2water} , we
 828 estimated the Takahashi’s Temperature/Biology ratio (Takahashi et al., 2002) to compare the
 829 influence of temperature and biological activities on pCO_{2water} . Across the 3 year period, we
 830 found that just $26.0 \pm 4.0\%$ (mean \pm SD) of forcing was attributable to **the effect of** temperature
 831 on solubility, confirming that the predominant driver of pCO_{2water} in the Rhode River is indeed
 832 biological activity (75%, Table 3). These patterns demonstrate the outsized role that biological
 833 processes play in shaping pCO_{2water} in nearshore marine and estuarine ecosystems (Dai et al.,
 834 2022; Van Dam et al., 2019).

Deleted:), a standardized approach

Deleted: -

835

836

837 **Table 3.** Takahashi Temperature/Biology Ratio (Eq. 5a From Takahashi et al. 2002).
 838

Deleted: JGR

Year	N	$\Delta p\text{CO}_2$ bio	$\Delta p\text{CO}_2$ temp	T/B ratio
2018	4416	3193.0	765.8	0.240
2019	8760	3669.8	1019.6	0.278
2020	8784	2772.1	846.0	0.305
2021	4345	2356.1	507.2	0.215
Overall	26305	3701.5	926.4	0.250

848
849850 3.5 Gas transfer velocity (k_{600})

851 Gas transfer velocity is affected by both mass transfer from molecular diffusion driven by ΔC
852 (i.e. CO_2 gradient between water and atmosphere) and momentum transfer linked to external
853 environmental forces that enhance turbulence at the air-water boundary layer (Ho et al., 2016;
854 Raymond & Cole, 2001; Van Dam et al., 2019). Van Dam et al. (2019) validated the use of wind
855 speed at 10 m above the water's surface (U_{10}) to estimate gas transfer velocities of CO_2 that were
856 standardized to a Schmidt number of 600 (k_{600}) by comparing estimated values to k_{600} values
857 derived directly from eddy covariance CO_2 flux measurements. Given the relative uniformity of
858 wind speed over the Rhode River where median binned U_{10} windspeed (converted from U_7
859 measurements) was $2.2 \text{ m} \cdot \text{s}^{-1}$ regardless of time of day or season, and that maximum values
860 rarely exceeded $10 \text{ m} \cdot \text{s}^{-1}$ (Table 1, Fig. S1), we chose to use the most conservative estuarine-
861 specific parameterization of k_{600} (Van Dam et al., 2019) (Eq. 2). The mean overall Rhode River
862 k_{600} value for CO_2 (mean \pm SD, $7.86 \pm 2.05 \text{ cm} \cdot \text{hr}^{-1}$) was of comparable magnitude to that of
863 the New River Estuary, NC ($9.37 \pm 9.47 \text{ cm} \cdot \text{hr}^{-1}$). However, wind speed varied far less on the
864 Rhode River than the New River estuary and day/night explained more variability in wind speed
865 than season. Because wind speed directly influenced the formulation of k_{600} (Eq. 2), the effect
866 size of day/night is similarly greater than the seasonal effect on gas transfer velocity (Table 2).
867 Nevertheless, effect sizes (ω^2) indicate that "season" explained at least 10 times more of the
868 observed variance of $p\text{CO}_2$ water, $p\text{CO}_2$ air, air-water concentration gradient, CO_2 flux, and gas-
869 specific solubility than "day/night" or their interaction (Table 2). Given the minor freshwater
870 input and microtidal nature of the Rhode River, we do not believe that lateral water velocity and
871 bottom turbulence appreciably affect the gas transfer velocity of CO_2 here, although we did not
872 investigate possible influences explicitly.

873

Deleted: 10m

Deleted: made in the New River Estuary, a shallow microtidal estuary similar to the Rhode River, which is applied here....

Deleted:). Effect

Deleted: than day/night

Deleted: JGR

880 Importantly, in coastal marine and estuarine habitats, ΔC can shift as much as several thousand
 881 μatm per day due to diel cycling associated with CO_2 production and depletion (Figs. 2, S2). The
 882 uncertainty surrounding gas transfer velocity parameterization can represent a major source of
 883 error in CO_2 flux calculations (Frankignoulle et al., 1998; Upstill-Goddard, 2006; Wanninkhof &
 884 McGillis, 1999); however, small errors in k_{600} have far less effect on CO_2 flux calculations in
 885 estuaries which experience $p\text{CO}_2$ swings of several thousand μatm during a single day, compared
 886 with more stable conditions of the open ocean where interannual ranges of $p\text{CO}_2$ are typically far
 887 less (Van Dam et al., 2019).

Deleted: and 3

888

889 3.6 CO_2 flux - Seasonality and Interannual Variation

890 CO_2 flux was determined according to Eq. 3 using hourly ΔC measurements, CO_2 solubility
 891 values (K_0) calculated according to temperature and salinity, and estuary-specific standardized
 892 gas transfer velocities (k_{600}) of Van Dam et al. (2019). CO_2 flux was plotted across the three
 893 years of observations at hourly and monthly intervals (Fig. 4a-b). As observed with $p\text{CO}_2$, CO_2
 894 flux in the Rhode River was shown to be strongly seasonal. Given the similarity in windspeed
 895 across seasons (Fig. S1), the effect of differential mean ΔC and variation between warm- and
 896 cold-water seasons (Fig. 2, Table 1) almost certainly drives the observed seasonal differences in
 897 CO_2 flux (Fig. 4). Again, the specific solubility of CO_2 is greatest at low temperatures, yet this is
 898 contrary to the observed mean $p\text{CO}_{2\text{water}}$ patterns, pointing toward a biological mechanism for
 899 $p\text{CO}_2$, ΔC , and ultimately, CO_2 flux. The effect size of season on CO_2 flux was two orders of
 900 magnitude greater than either day/night or the season day/night by interaction (Table 2).

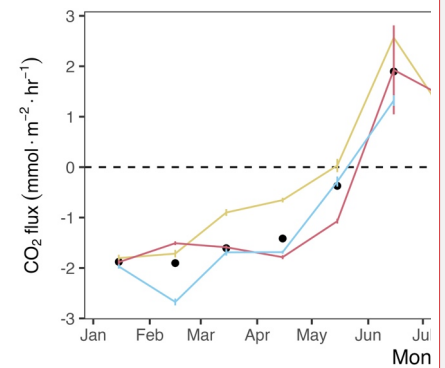
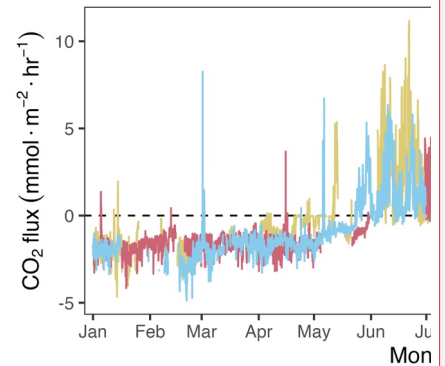
Deleted: 5a

Deleted: apparent

Deleted: 5

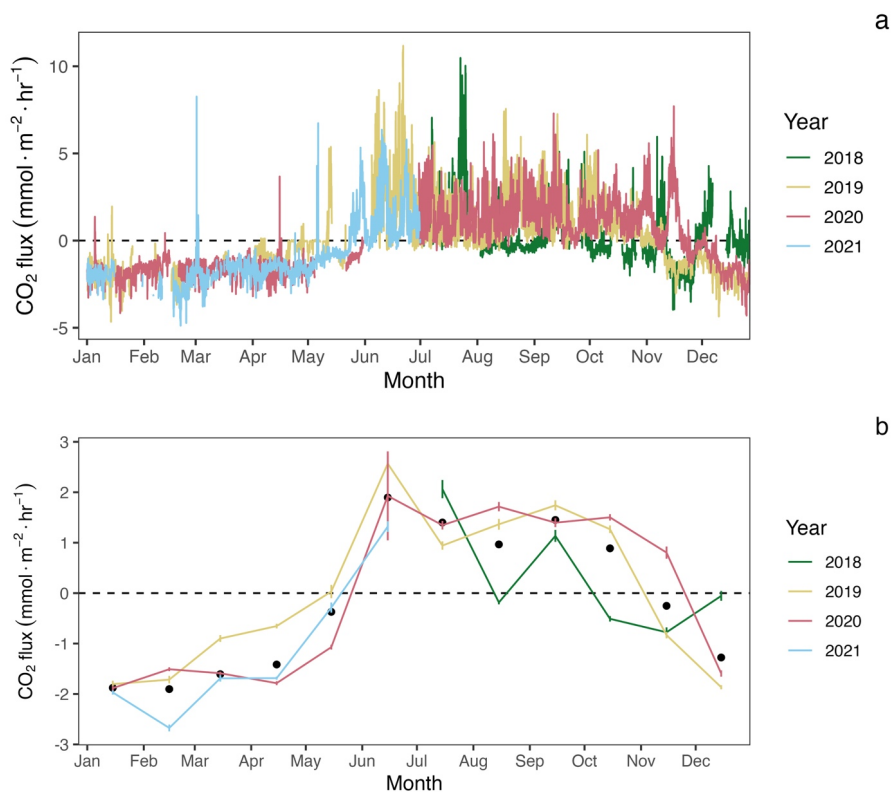
Deleted: by

Deleted:



Deleted: JGR

908



909

910 **Fig. 4.** CO₂ flux estimates by year: a. Hourly, b. Monthly average CO₂ flux estimates with 95%
 911 confidence limits. Black dots in panel b indicate mean monthly fluxes across years.

Deleted: 5

912 Among years, $p\text{CO}_{2\text{water}}$ and CO₂ flux largely repeat themselves, with dissolved CO₂ becoming
 913 consistently sub-atmospheric and CO₂ flux going negative (gas exchange from atmosphere to
 914 water) between December and May and abruptly transitioning to much higher maximum, yet
 915 variable $p\text{CO}_{2\text{water}}$ values with net positive CO₂ fluxes from June through November (Figs. 2 and
 916 4). Monthly averaged CO₂ fluxes are consistent among years (Fig. 4b), with net positive CO₂
 917 fluxes (heterotrophic conditions) between June and November and negative (autotrophic) fluxes
 918 dominating when water temperatures are cold, between December and May. Despite the overall
 919

Deleted: 1

Deleted: 5

Deleted: 5b

Deleted:

Deleted: JGR

925 similarities in seasonal CO₂ flux, inter-annual patterns can vary considerably. When hourly CO₂
926 flux values were averaged for the year, the Rhode River in 2019 was shown to have a net
927 positive flux but a net negative flux in 2020. When scaled for the year, 2019 outgassed CO₂ from
928 the water to the atmosphere at a rate of 2215.08 mmol · m⁻² · yr⁻¹ (95% CI = 1816.88, 2613.29).
929 The annual net flux rate in 2020 was negative (i.e. CO₂ moved from the atmosphere into the
930 river) at a rate of -1361.31 mmol · m⁻² · yr⁻¹ (95% CI = -1723.60, -999.01).

931

932 At shorter time scales, such as comparing the same week of the year among years, we sometimes
933 observed vast differences in the magnitude and direction of CO₂ flux (Fig. S3), signaling
934 differences in seasonal conditions between years. Transient events can also result in deviations
935 from otherwise typical CO₂ flux conditions. For example, the period from July 2018 to Jan 2019
936 deviated from other years as CO₂ flux was more erratic, with intermittent periods of negative and
937 positive CO₂ flux extending later into the winter season than in other years. When water
938 temperatures are compared among years, 2018 was shown to be more inconsistent, with more
939 pronounced temperature shifts and reversals than in 2019 or 2020 (Fig. S1). Salinities remained
940 relatively low for the latter half of 2018 into early 2019, reflecting wetter conditions (Fig. S1).
941 There were also two rapid salinity declines (>4 ppt reductions) in July and October 2018, likely
942 associated with strong precipitation events. These events were both followed by immediate
943 spikes in chlorophyll-*a* concentration to levels exceeding 200 µg · L⁻¹, indicative of
944 phytoplankton bloom conditions. From 2018 to 2021, chlorophyll-*a* levels of this magnitude and
945 greater were generally confined to cold-water months (Dec–May; Fig. S1 Erratic water
946 temperature and salinity are also reflected in more variable gas-specific solubility (*K*₀) for CO₂ in
947 2018 than later years (Fig. 3).

948

949 Gallegos et al. (1992) documented predictable phytoplankton blooms associated with freshets in
950 the Rhode River, when nutrient-rich freshwater inundates the estuary, not from point and non-
951 point sources within the local Rhode River watershed, but instead from the enormous watershed
952 that feeds the Susquehanna River, the primary source of freshwater input into the Chesapeake
953 above the Potomac as well as >50% of the entire Bay's freshwater (U.S. Geological Survey,
954 2023). Unlike river dominated estuaries, in the Rhode River estuary, volumetric influxes from
955 the Chesapeake Bay end member far exceed freshwater input from the Muddy Creek and

Deleted: S2

Deleted: across

Deleted: and

Deleted: 4

Deleted: JGR

960 secondary tributaries. In the Rhode River, phytoplankton blooms result in the temporary
 961 depletion of $p\text{CO}_{2\text{water}}$, followed by a spike, as phytoplankton senesce and organic carbon is
 962 decomposed/re-mineralized back into inorganic carbon. Episodic, short-lived occurrences like
 963 these demonstrate how immediate small scale biological forcing, can be coupled with, and
 964 catalyzed by, distant large-scale weather and hydrological events. These in turn can influence
 965 $p\text{CO}_2$ flux variations within seasons and among years (Fig. 3 and S3; and Chen et al., 2020).

Deleted: 5

Deleted: S2

967 Overall, except for wind speed, the effect sizes for the other six measured or calculated variables
 968 were shown to be greatest for season vs. day/night or the interaction of season x day/night, and in
 969 all cases the season effect was greater by at least 1 order of magnitude (Table 2). Seasonality has
 970 10 to 1000 times more explanatory power than other variables investigated as estimated by ω^2
 971 (Table 2).

973 3.7 Diel Cycling

974 The notion that estuaries are predominantly heterotrophic systems that invariably outgas more
 975 CO_2 to the atmosphere than they absorb has been a long-held view (Abril et al., 2000; Borges et
 976 al., 2004; Cai, 2011; Cai et al., 2000; Chen, 2013; Frankignoulle et al., 1998, Gattuso et al.,
 977 1998). However, more recently investigators have realized that physical and hydrological
 978 characteristics, geographical location, size, and biological and biogeochemical activities may
 979 individually, or together, influence CO_2 flux in estuaries and therefore contributions to
 980 atmospheric chemistry (Brodeur et al. 2019; Caffrey, 2004; Chen et al., 2013, 2020; Herrmann et
 981 al., 2020). Furthermore, inadequate sampling can induce bias (e.g., upscaling from a small
 982 number of daytime samples taken during warm-water months can skew apparent patterns;
 983 Laruelle et al., 2017; Van Dam et al., 2019.) Using 1-minute sampling intervals, averaged to the
 984 hour, reveals patterns in the Rhode River that might otherwise be overlooked. We document the
 985 Rhode River as having strong seasonality in both $p\text{CO}_2$ content as well as the extent and
 986 direction of CO_2 flux (Figs. 2, S1, S2). Both measures are marked by daily oscillations,
 987 frequently reversing direction during a single 24-hr period in warm-water months (Figs. 2) but
 988 more stable and unidirectional during cold-water months (Figs. 2 and 5).

Deleted: -

Deleted: continually over three years

Deleted: and 3

Deleted: the CO_2 gradient (ΔC)

Deleted: -

Deleted: and 3

Deleted: are

990 3.8 Shifting Net Ecosystem Production

Deleted: JGR

1000 To better understand how the net ecosystem production (NEP) of the Rhode River shifts
1001 throughout the year, where positive NEP indicates the river is storing carbon (autotrophic state)
1002 and negative NEP indicates it is releasing carbon to the atmosphere (heterotrophic state), we
1003 calculated hourly CO₂ flux values, averaged them by day (i.e. 24 hr period) and plotted each in
1004 relation to the ΔC = 0 reference. Each day of the 3 yr study was categorized as either net
1005 heterotrophic (CO₂ flux from water to atmosphere) or net autotrophic (CO₂ flux from atmosphere
1006 to water). Each day was then further identified as either purely heterotrophic (all 24 hours were
1007 heterotrophic), purely autotrophic, or mixed (some hours were heterotrophic and some were
1008 autotrophic but resulting in a net autotrophic or net heterotrophic state for the day) (Fig. 5). From
1009 July 2018 to July 2021, most 24 hr periods were categorized as pure autotrophic (444/920 =
1010 48%), while 25% (229/990) were purely heterotrophic, and the remainder of mixed trophic status
1011 (17% net heterotrophic and 10% net autotrophic; Fig. 5).

Deleted: and

Deleted: -

Deleted: Every given

Deleted: -

Deleted: ,

Deleted: 6

Deleted: -

Deleted: .3

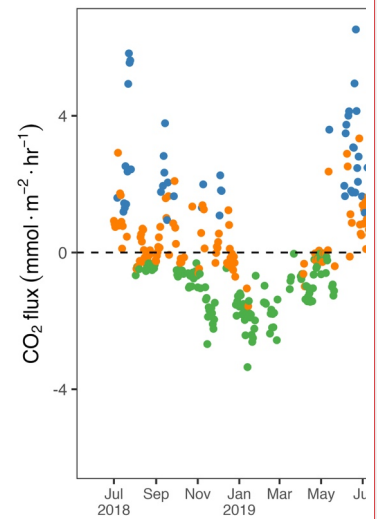
Deleted: 24.9

Deleted: .0

Deleted: .0

Deleted: 6).

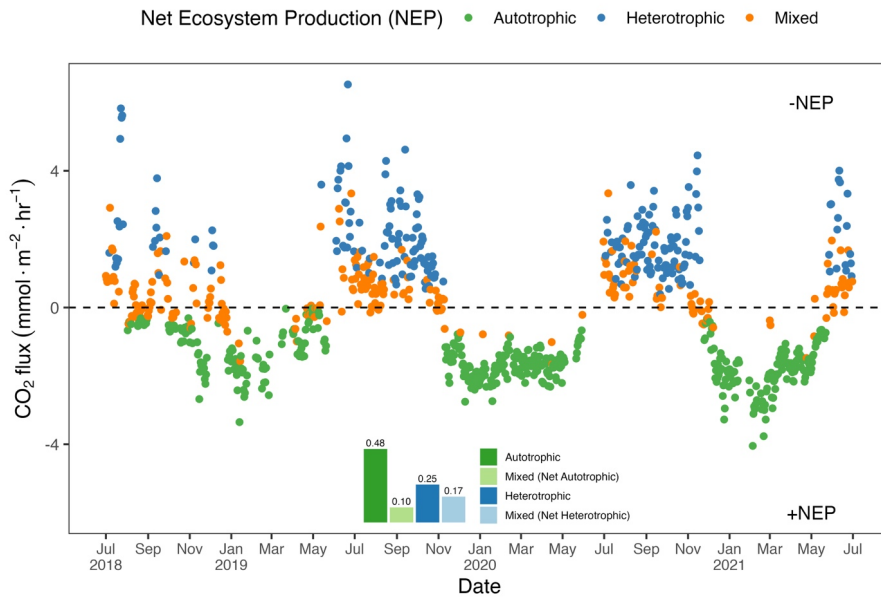
Net Ecosystem Producti



Deleted:

Deleted: JGR

1027



1028

1029 **Fig. 5.** Daily mean CO₂ flux estimates (CO₂ gradient is CO_{2water} – CO_{2air}). Green dots indicate
 1030 days when all 24 hourly flux measurements were negative (autotrophic with +NEP); blue dots
 1031 indicate days on which all 24 hourly flux measurements were positive (heterotrophic with -NEP).
 1032 Orange dots indicate that hourly fluxes were both negative and positive, and the position of the
 1033 orange dot below or above the zero line indicates whether the day was net autotrophic or net
 1034 heterotrophic. Inset describes the proportion of days in each category indicating that during 58%
 1035 (0.48 + 0.10) of days across three years of observation, the Rhode River was a CO₂ sink.

Deleted: 6

Deleted: on which

Deleted:) and orange

Deleted: or

Deleted:

1036

1037 Altogether, the Rhode River was net autotrophic for (535 of 920 days = 58%) and net
 1038 heterotrophic for 42% (385 days) across three years. When CO₂ flux is integrated over all three
 1039 years, the Rhode River is shown to have near neutral NEP (Fig. 6). The effect size of season is
 1040 two orders of magnitude greater than either that of day/night or season:day/night interaction
 1041 (Table 2). Mean CO₂ flux values highlight the obvious correlation between season and NEP;
 1042 error bars (± 1 SD) reveal the importance of diel cycling where the magnitude and directionality
 1043 of day/night flux variability is approximately equal to the overall variability accrued across all
 1044 three years (Fig. 6). Although CO₂ flux is less variable and more autotrophic during cold-water

Deleted: .2

Deleted: 41.8

Deleted: However, because CO₂ flux is integrative, it is vital to know the magnitude and direction of flux to understand the nature of the river's NEP.

Deleted: summarized across

Deleted: 3

Deleted: according to season and day/night cycles,

Deleted: estuary

Deleted: slightly autotrophic;

Deleted: 7

Deleted: Day/Night

Deleted: 7

Deleted: JGR

1063 months than warm-months in the Rhode River, the range of possible values that occur across
 1064 night and day, regardless of season, must be taken into consideration to minimize incidental
 1065 sampling bias (Figs. 2 and 6).

Deleted: 7

1067 A multi-year investigation of CO₂ flux in the main stem of Chesapeake Bay by Chen et al.
 1068 (2020) combined several bay-wide cruises that were distributed across seasons to collect discrete
 1069 and underway pCO₂ data for CO₂ flux calculations. They concluded that the low salinity upper
 1070 bay, which receives large volumes of freshwater from the Susquehanna River, was net
 1071 heterotrophic; the mesohaline middle bay was net autotrophic, and the polyhaline lower bay was
 1072 near carbon neutral. Chen et al. (2020) characterized Chesapeake Bay, on the whole, as a weak
 1073 source of CO₂ to the atmosphere (net flux = 0.73 mol · m⁻² · yr⁻¹) but suggested that during wet
 1074 years, it may function as weak sink of CO₂. Herrmann et al. (2020) also concluded that the
 1075 Chesapeake Bay was a weak source of CO₂ to the atmosphere based on calculated pCO₂ values
 1076 from long term pH and alkalinity measurements (net flux = 1.2 mol · m⁻² · yr⁻¹mol). Brodeur and
 1077 colleagues (2019) examined dissolved inorganic carbon (DIC) and total alkalinity along the
 1078 mainstem of the Chesapeake Bay across the year in 2016 and concluded that DIC increases from
 1079 north to south and from surface waters to depth, but that seasonal riverine input and biological
 1080 cycling were significantly important, concluding that the Bay as a whole was a sink for CO₂.

Deleted: DIC

Deleted: and

Deleted: , but that

Deleted: may be

Deleted: net

Deleted: of

1082 When our annual mean pCO₂ values were compared with the Chen et al. (2020) survey, the
 1083 Rhode River was shown to be higher on average and more variable than the mesohaline main
 1084 stem of the Bay (591 ± 652 vs. 416 ± 167 μatm), including a substantially greater measured
 1085 range (min = 15, max = 5182 μatm vs. 103 and 1033 μatm). These results suggest that water in
 1086 the shallow and well mixed Rhode River, and DIC in particular, undergo more acute biological
 1087 transformation than in the mesohaline main stem of Chesapeake Bay. Chen et al. (2020) point to
 1088 a variety of factors that affect pCO₂ and CO₂ flux in the main stem bay, including temperature,
 1089 depth, stratification, and freshwater input volume, some of which may attenuate biological
 1090 forcing. Interannual variability was demonstrated in both the Rhode River (some years were net
 1091 autotrophic and others heterotrophic, Figs. 4 and 5) and in the mesohaline main stem of the Bay;
 1092 however, we attribute interannual variability in pCO₂ and CO₂ flux primarily to variation in
 1093 water temperature that in turn drives biological activity. We conclude that seasonal variations the

Deleted: b

Deleted: dissolved inorganic carbon (DIC)

Deleted: 5

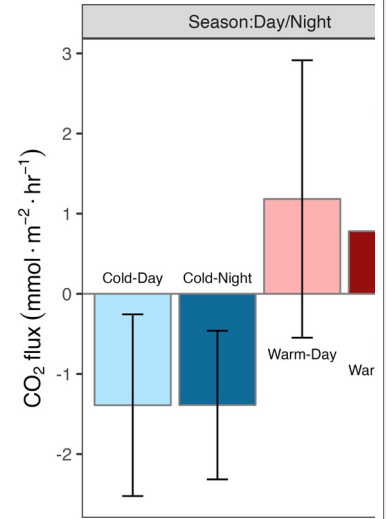
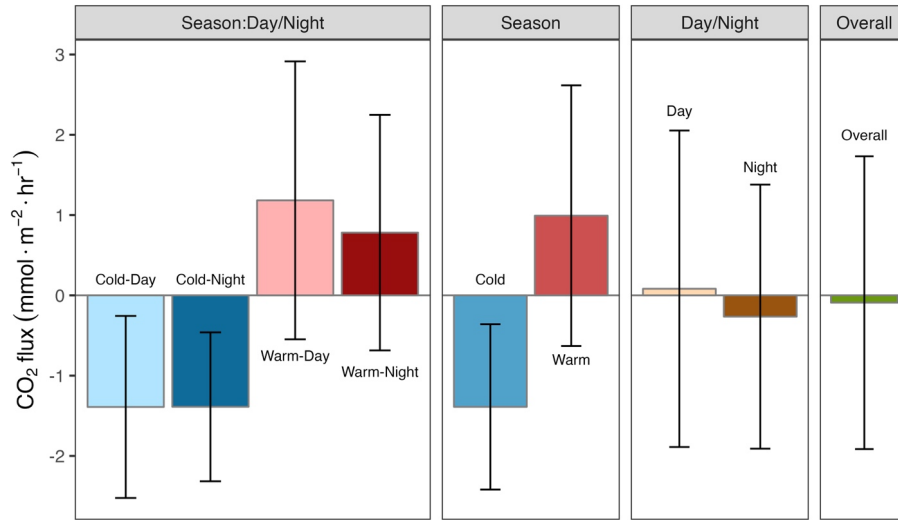
Deleted: 6

Deleted: b

Deleted: JGR

1106 Rhode River (and likely similar rivers in the mesohaline portion of the Chesapeake) are
 1107 significant and predictable, closely associated with water temperature, **and that temperature**
 1108 mediates NEP biologically rather than by changes to the solubility of CO₂.

Deleted: but as



Deleted:

1109
 1110

1111 **Fig. 6.** Mean CO₂ flux ± 1 SD (mmol · m⁻² · hr⁻¹) plotted by day/night cycling, cold-water/warm-
 1112 water season, season by day/night interaction, and overall CO₂ flux across three years of
 1113 observation.

Deleted: 7

1115 In the Rhode River, we find that CO₂ flux reverses itself daily for part of the year (June–
 1116 November) yielding some days that are characterized as a net sink (net autotrophic) and others
 1117 that are a net source (net heterotrophic). From December to May, diel cycling is minimal and the
 1118 river is almost exclusively a net sink, autotrophic both day and night. Finally, although CO₂ flux
 1119 is pronounced but variable across seasons, the net CO₂ flux of the Rhode River on an annual
 1120 basis is near neutral.

Moved (insertion) [1]

Moved (insertion) [2]

1121
 1122
 1123

Formatted: Font: +Headings CS (Times New Roman), Not Bold, Underline

1124 3.9 Lateral transport

Deleted: JGR

1128 Tidal cycling has been shown to liberate and laterally transport DOC from brackish marshes to
1129 adjacent estuaries (Cai, 2011; Herrmann, 2015) and therefore is of great importance to carbon
1130 cycling and budgets of wetlands and estuaries (Najjar et al., 2020). DOC outwelling from the
1131 Kirkpatrick Marsh (hereafter KPM), a 0.21 km² tidal marsh located approximately 1 km up
1132 estuary from our primary study site at the SERC Dock (Fig. 1), into the Rhode River has been
1133 measured and modeled extensively in recent years (Clark et al., 2020; Menendez et al., 2022;
1134 Tzortziou et al., 2011; Tzortziou et al., 2008). These studies indicate that the KPM is responsible
1135 for a large portion of overall DOC input to the Rhode River, as well as significant export from
1136 the river to the mainstem of Chesapeake Bay. Model generation and validation by Clark et al.
1137 (2020) indicate that up to 13.1% of the total DOC input to the Rhode River originates in the
1138 KPM. Another important source (53% of total) is DOC derived from phytoplankton and is
1139 therefore labile and readily biodegraded and remineralized into DIC. Furthermore, large
1140 quantities of other, semi-labile forms of DOC are exported from the KPM, which are themselves
1141 subject to photochemical and biodegradation and remineralization (Clark et al., 2020).
1142 Importantly, each of these DOC streams provides a potential source of DIC, including $p\text{CO}_2$, to
1143 the Rhode River.

Deleted: -ha

Deleted:)

1144
1145 Dissolved inorganic carbon generated in brackish tidal wetlands is also outwelled directly into
1146 estuaries (e.g., Cai et al., 2000; Chu et al., 2018; Song et al., 2023). Recent work by Song et al.
1147 (2023) demonstrates that $p\text{CO}_2$ in a salt marsh tidal creek in Waquoit Bay, MA was regulated by
1148 both tide height (inversely) and the day/night cycle, with nighttime low tides resulting in the
1149 highest $p\text{CO}_2$ values, signaling a strong local effect from respiration and photosynthesis in
1150 combination with tidal outwelling.

1151
1152 In the Rhode River watershed $p\text{CO}_2$ was measured continuously in the single tidal creek that
1153 drains the KPM using the same methods as at our primary study location. We observed that the
1154 KPM tidal creek $p\text{CO}_2$ follows the tidal cycle exclusively, yet outside the mouth of the tidal
1155 creek, in the estuary proper, day/night cycling overwhelms this marsh tidal signal. Simultaneous
1156 $p\text{CO}_2$ measurements from the SERC dock follow a strict day/night cycle (Fig. S4). However,
1157 while peak levels of dissolved CO_2 in the Kirkpatrick Marsh creek occur at low tide and can
1158 reach values nearly 20 times greater than highs at the SERC dock (Fig. S4) there is no obvious

Deleted: s

Deleted: S3

Deleted: S3

Deleted: JGR

1164 evidence of this tidal DIC input at the dock site. Remineralization of DOC exported from the
 1165 KPM, as well as DOC originating in other locations within the watershed are important sources
 1166 of DIC in the river, but given the relative volumes of these sources to that of the much larger
 1167 estuary, as well as the physical distance (~1 km) from SERC dock, these input signals should be
 1168 expected to be lagged and damped inside the estuary and not tightly coupled with tidal cycles.
 1169 Instead, $p\text{CO}_2$ exported from the KPM is expected to undergo significant dilution effects, be
 1170 partially off-gassed to the atmosphere, and be metabolized via photosynthesis, reducing its
 1171 influence on downstream sites. These findings suggest that despite periodic extreme $p\text{CO}_2$ in
 1172 KPM tidal creek (>30,000 ppmv), the overall mass of CO_2 export is not sufficient to have
 1173 measurable effects on the deeper, well-mixed portions of the Rhode River.

Deleted: These findings suggest that despite periodic extreme CO_2 concentrations (>25,000 ppmv), the overall mass of CO_2 export is not sufficient to have an immediate, measurable effects on the deeper, well-mixed portions of the Rhode River.

Formatted: Pattern: Clear

Deleted: .

1175 Thus, although land-sea interfaces and outwelling of DOC and DIC are important in estuaries
 1176 and coastal ecosystems, the relative sizes of wetlands and adjacent water bodies and the overall
 1177 volume of water moving between the two are also important factors. In eutrophic estuaries like
 1178 the Rhode River, biological forcing can rapidly assimilate DIC and degrade and mineralize labile
 1179 forms of DOC, as evidenced by extensive diel cycling in these systems (e.g., Brodeur et al. 2019;
 1180 Song et al. 2023, and the present study.) The much larger and complex Chesapeake Bay
 1181 generally follows seasonal changes in $p\text{CO}_2$ and CO_2 flux, but these appear to be most
 1182 predictable in the upper oligohaline portion and the polyhaline region of the bay near the mouth,
 1183 where freshwater and oceanic end-member effects are most pronounced (Brodeur et al. 2019;
 1184 Chen et al., 2020). The central mesohaline part of Chesapeake Bay comprises numerous discrete
 1185 and unique watersheds and subestuaries/rivers, each of which exchanges water with the bay.
 1186 Elucidating spatial and temporal patterns of $p\text{CO}_2$ and CO_2 flux are vital for understanding each
 1187 one's role as an atmospheric source or sink, but also could provide better insight into how each
 1188 may be influenced by global increases in atmospheric CO_2 (i.e., acidification and its influences
 1189 on estuarine metabolism, and the local biota, fisheries, and habitats each support.) Collectively,
 1190 these and other subestuaries will have cumulative effects on the overall water quality of
 1191 Chesapeake Bay, including cycling of DOC and DIC, which in turn affect $p\text{CO}_2$ and CO_2 flux.

Deleted: -

1193 4. Conclusion

Deleted: and Recommendations

Deleted: JGR

1203 As indicated in this study and others, the role that biological processes play in estuaries to either
 1204 fix CO₂ (autotrophy) or liberate CO₂ (heterotrophy) are extensive, complex, and can be quite
 1205 variable over space and time (Brodeur et al. 2019; Chen et al., 2020; Herrmann et al., 2020;
 1206 Rosentreter et al., 2021). High frequency automated measurements revealed strong seasonal
 1207 contrasts in dissolved CO₂ content and CO₂ flux between water and atmosphere of the Rhode
 1208 River, a shallow mesohaline reach of the Chesapeake Bay. Importantly, only through high
 1209 frequency, multi-year measurements could diel and seasonal cycling be fully discerned. The
 1210 timing and frequency of measurements are critical and have potential for strong and misleading
 1211 biases if sampling is insufficient. In contrast, cold-water months coincide with long periods
 1212 (weeks to months) of continuous sub-atmospheric sink conditions for CO₂. Using these
 1213 measurements, we estimated the direction and magnitude of CO₂ flux in hourly, daily, and
 1214 annual terms. In the Rhode River CO₂ flux reverses itself daily for part of the year (June through
 1215 November) yielding some days that are characterized as net sink (net autotrophic and NEP > 0)
 1216 and others that are net source (net heterotrophic and NEP < 0). From December to May diel
 1217 cycling is minimal, and the river is almost exclusively a CO₂ sink with +NEP both day and night.
 1218 Although CO₂ flux is pronounced but variable across seasons, the net CO₂ flux of the Rhode
 1219 River on an annual basis is near carbon neutral, although some years are net heterotrophic and
 1220 others net autotrophic.

Deleted: Jun–Nov

Deleted: the river has negative

Deleted: Dec–

Deleted: /net autotrophic

1221
 1222 High frequency sampling of *p*CO₂, although typically confined spatially, is one approach to
 1223 understanding fundamental aspects of estuarine metabolic states and CO₂ flux that may
 1224 otherwise go undetected (Song et al., 2023). To address the spatial complexity of estuarine,
 1225 nearshore, and inland waters, more observation locations are required. As with any
 1226 environmental or ecological question, careful sampling design is critical to balance efficiency
 1227 and statistical power.

1228
 1229 As the largest and arguably most complex estuary in the United States, the Chesapeake Bay is
 1230 the subject of extensive ecosystem management efforts and ranks among the most studied and
 1231 monitored estuaries in the world (Boesch and Goldman 2009). Yet, information on CO₂ and
 1232 GHG fluxes continue to be limited (Brodeur 2019; Chen et al., 2020; Herrmann et al., 2020).
 1233 Given the extensive coordinated monitoring programs that either make real-time water quality

Formatted: No underline

Deleted: greenhouse gas flux continues

1239 measurements and/or maintain routine water sampling schedules (e.g., Maryland DNR “Eyes on
 1240 the Bay” program) in this region, ~~existing~~ water quality observation assets and sampling
 1241 programs could be ~~leveraged~~ to more fully characterize and quantify CO₂ and other ~~GHG~~
 1242 dynamics and flux in the Bay and elsewhere (see Saba et al. 2019). For example, coordinated
 1243 deployment of additional automated sampling devices (e.g., robust air-water equilibrators and
 1244 traditional atmospheric gas sensors) in key locations would enable estimates of CO₂ flux, and if
 1245 combined with pH, DIC, or total alkalinity measurements, carbonate chemistry calculations as
 1246 well. Importantly, such installations need not be permanent. Instead, a small group of
 1247 instruments could be systematically deployed across an existing observation network, co-located
 1248 with other water quality instruments using a stratified sampling approach to capture spatial
 1249 variability. For example, a set of shifting two ~~to four~~ week ~~deployments~~ during summer and
 1250 winter months could yield sufficient data to advance our understanding of Chesapeake Bay-wide
 1251 CO₂ flux significantly in a single year. Such information would complement underway transects
 1252 that are vital, but which tend to underestimate temporal variability in any given location. In the
 1253 case of dissolved ~~GHGs~~, liquid-air equilibration techniques are being used to measure multiple
 1254 ~~GHGs~~ (Call et al. 2015; Hartmann, 2018; Gülzow et al. 2011; Miller et al. 2019; Xiao et al.
 1255 2020).
 1256
 1257 Understanding the ~~GHG~~ dynamics in estuaries is a vital component to generating accurate global
 1258 budgets (Maher & Eyre, 2012) as well as informing where emerging carbon capture
 1259 technologies, ~~including nature-based solutions~~, might be best located (Bradshaw & Dance, 2005;
 1260 Sun et al., 2021). In the case of estuaries, there have been extensive global losses of seagrasses
 1261 due to habitat degradation, pollution, and disease (Waycott et al. 2009). In addition to many
 1262 other ecosystem service benefits, restoration of seagrass and submerged aquatic vegetation has
 1263 the potential to restore and enhance natural carbon sequestration (i.e. blue carbon; Kennedy et al.
 1264 2022; Macreadie et al. 2022; Unsworth et al. 2022). ~~In Virginia, U.S.A., Oreska et al. (2020)~~
 1265 ~~demonstrated how the functional benefits of a restored seagrass meadow habitat can be~~
 1266 ~~quantified ecologically in terms of their ability to sequester carbon and affect GHG fluxes~~
 1267 ~~between the estuary and atmosphere. Uniquely, these investigators then monetized the costs and~~
 1268 ~~benefits of habitat restoration and function as CO₂ offset credits, as part of a GHG budget, and~~

Deleted: JGR

Deleted: strategic leveraging of

Deleted: achieved

Deleted: /or

Deleted: greenhouse gas

Deleted: -

Deleted: to 1-month long

Deleted: greenhouse gases

Deleted: greenhouse gas gases

Formatted: No underline

Deleted: greenhouse gas

Deleted:), including nature-based solutions.

Deleted: In an increasingly automated world, marrying innovative, robust, and economical measurement solutions with traditional observing networks will provide efficient, real-time information that can be readily shared. Such information will increase our understanding of greenhouse gas flux at both the local habitat scales that are of local ecological significance, as well as at the ecosystem level of an estuary.

1287 demonstrated how such approaches can be used to incentivize habitat restoration (Oreska et al.
1288 (2020).

1289
1290 Increasing the completeness and utility of global GHG budgets, as they relate to human activities
1291 and ecosystem functions, are necessary steps toward combating global climate change.
1292 Measurement of GHGs at high spatial and temporal resolution using economical, automated
1293 measurement solutions can increase our understanding of GHG dynamics at small ecologically
1294 significant scales, as well as at the larger ecosystem level of an estuary.

1295

1296 **Data Availability**

1297 Hourly means of pCO₂ and associated environmental data used in the analyses are available at
1298 the Smithsonian Figshare repository <https://doi.org/10.25573/serc.22491655> via under Creative
1299 Commons license CC BY-NC 4.0.

1300

1301 **Author Contributions**

1302 AWM contributed to project Conceptualization, Funding acquisition, Investigation,
1303 Methodology, Project Administration, Resources, Supervision and Writing – Original Draft.
1304 JRM contributed to Data Curation, Formal Analysis, Software and Visualization. ACR
1305 contributed to Data Curation, Investigation, Methodology and Project Administration. MSM
1306 contributed to Conceptualization, Supervision and Visualization. KJK contributed to
1307 Conceptualization, Data Curation, Software, Validation. All authors contributed to Writing –
1308 review and editing.

1309

1310 **Competing Interests**

1311 The corresponding author has declared that none of the authors has any competing interests.

1312

1313

Formatted: Font: Times New Roman, Not Bold

1314

Formatted: Line spacing: 1.5 lines

1315

Deleted: JGR

1316 Acknowledgments

1317 We thank Patrick Neale and Stephanie Wilson for their early review and critical feedback on this
1318 manuscript, as well as J. Patrick Megonigal for discussions on methodology and two anonymous
1319 reviewers who contributed beneficial suggestions. Funding for this research was provided by the
1320 Smithsonian Institution.

Deleted: wish to...thank Patrick Neale and Stephanie Wilson for their early review and critical feedback on this manuscript, as well as J. Patrick Megonigal for discussions on methodology. ... [561]

Formatted: Line spacing: 1.5 lines

Formatted: Font: Bold

1322 References

1323 Abril, G. and Borges, A. V.: Carbon Dioxide and Methane Emissions from Estuaries, in:
1324 Greenhouse Gas Emissions — Fluxes and Processes: Hydroelectric Reservoirs and Natural
1325 Environments, edited by: Tremblay, A., Varfalvy, L., Roehm, C., and Garneau, M., Springer,
1326 Berlin, Heidelberg, 187–207, https://doi.org/10.1007/978-3-540-26643-3_8, 2005.

Deleted: Open Research
AGU requires an Availability Statement for the underlying data needed to understand, evaluate, and build upon the reported research at the time of peer review and publication. Additionally, authors should include an Availability Statement for the software that has a significant impact on the research. Details and templates are in the [Availability Statement](#) section of the Data & Software for Authors Guidance. For physical samples, use the IGSN persi... [562]

Formatted: Font: Not Bold, Not Highlight

Deleted: ¶ ... [563]

Formatted: Font: Not Italic

1327 Abril, G., Etcheber, H., Borges, A. V., and Frankignoulle, M.: Excess atmospheric carbon
1328 dioxide transported by rivers into the Scheldt estuary, Comptes Rendus de l'Académie des
1329 Sciences - Series IIA - Earth and Planetary Science, 330, 761–768,
1330 [https://doi.org/10.1016/S1251-8050\(00\)00231-7](https://doi.org/10.1016/S1251-8050(00)00231-7), 2000.

Deleted: (pp. 187–207)... edited by: Tremblay, A. ... [564]

Deleted: &...nd Frankignoulle, M. (2000)...: Excer... [565]

Deleted: D

Formatted: Font: Not Italic

Formatted ... [566]

Deleted: (11),... 761–768. ... [567]

Formatted: Not Highlight

1331 Bauer, J. E., Cai, W.-J., Raymond, P. A., Bianchi, T. S., Hopkinson, C. S., and Regnier, P. A. G.:
1332 The changing carbon cycle of the coastal ocean, Nature, 504, 61–70,
1333 <https://doi.org/10.1038/nature12857>, 2013.

Deleted: ¶ ... [568]

Formatted ... [569]

Deleted: (7478),... 61–70. ... [570]

1334 Benson, S., Rich, R., Tashjian, A., Lonneman, M., and Neale, P.: MarineGEO Upper
1335 Chesapeake Bay Observatory CPOP Data, <https://doi.org/10.25573/SERC.C.6100368.V10>,
1336 2023.

Deleted: ¶ ... [571]

Deleted: ¶

Deleted: (2009).

Deleted: b

Deleted: In K. McLeod and H. Leslie (Eds.)

1337 Boesch, D.F. and Goldman, E.B.: Chesapeake Bay, USA, in: Ecosystem-Based Management for
1338 the Oceans, edited by: McLeod, K. McLeod and Leslie H. Island Press, Washington, D.C., 268–
1339 293, 2009.

Formatted: No underline, Font color: Text 1

Formatted: No underline, Font color: Text 1

Formatted: No underline, Font color: Text 1

Formatted ... [572]

Deleted: (2009), pp.

Deleted: -

Formatted: Font color: Text 1

1341 Borges, A. V.: Do we have enough pieces of the jigsaw to integrate CO2 fluxes in the coastal
1342 ocean?, Estuaries, 28, 3–27, <https://doi.org/10.1007/BF02732750>, 2005.

Formatted ... [573]

Deleted: ¶ ... [574]

Deleted: (1),... 3–27. ... [576]

Formatted ... [575]

1450 Borges, A. V., Delille, B., Schiettecatte, L.-S., Gazeau, F., Abril, G., and Frankignoulle, M.: Gas
 1451 transfer velocities of CO₂ in three European estuaries (Randers Fjord, Scheldt, and Thames),
 1452 *Limnology and Oceanography*, 49, 1630–1641, 2004.

1453 Bradshaw, J. and Dance, T.: Mapping geological storage prospectivity of CO₂ for the world’s
 1454 sedimentary basins and regional source to sink matching. in: *Greenhouse Gas Control
 1455 Technologies 7*, vol. I, Elsevier, 583–591, <https://doi.org/10.1016/B978-008044704-9/50059-8>,
 1456 2005.

1457 Breitbart, D. L., Hines, A. H., Jordan, T. E., McCormick, M. K., Weller, D. E., and Whigham,
 1458 D. F.: Landscape patterns, nutrient discharges, and biota of the Rhode River estuary and its
 1459 watershed: Contribution of the Smithsonian Environmental Research Center to the Pilot
 1460 Integrated Ecosystem Assessment, 2008.

1461 Brodeur, J. R., Chen, B., Su, J., Xu, Y.-Y., Hussain, N., Scaboo, K. M., Zhang, Y., Testa, J. M.,
 1462 and Cai, W.-J.: Chesapeake Bay Inorganic Carbon: Spatial Distribution and Seasonal Variability,
 1463 *Frontiers in Marine Science*, 6, <https://doi.org/10.3389/fmars.2019.00099>, 2019.

1464 Broecker, W. S., Takahashi, T., Simpson, H. J., and Peng, T.-H.: Fate of Fossil Fuel Carbon
 1465 Dioxide and the Global Carbon Budget, *Science*, 206, 409–418, 1979.

1466 Caffrey, J. M.: Factors controlling net ecosystem metabolism in US estuaries, *Estuaries*, 27, 90–
 1467 101, 2004.

1468 Cai, W.-J.: Estuarine and Coastal Ocean Carbon Paradox: CO₂ Sinks or Sites of Terrestrial
 1469 Carbon Incineration?, *Annual Review of Marine Science*, 3, 123–145,
 1470 <https://doi.org/10.1146/annurev-marine-120709-142723>, 2011.

1471 Cai, W.-J. and Wang, Y.: The chemistry, fluxes, and sources of carbon dioxide in the estuarine
 1472 waters of the Satilla and Altamaha Rivers, Georgia, *Limnology and Oceanography*, 43, 657–668,
 1473 <https://doi.org/10.4319/lo.1998.43.4.0657>, 1998.

1474 Cai, W.-J., Wiebe, W. J., Wang, Y., and Sheldon, J. E.: Intertidal marsh as a source of dissolved
 1475 inorganic carbon and a sink of nitrate in the Satilla River-estuarine complex in the southeastern
 1476 U.S., *Limnology and Oceanography*, 45, 1743–1752, <https://doi.org/10.4319/lo.2000.45.8.1743>,
 1477 2000.

Deleted: JGR

Deleted: ¶ [577]

Deleted: (5),... 1630–1641. [579]

Formatted [578]

Deleted: ., &... and Dance, T. (2005),...: Mapping geological storage prospectivity of CO₂ for the world’s sedimentary basins and regional source to sink match[... [580]

Formatted: Font: Not Italic

Deleted: (V...ol. I, pp...lsevier, 583–591). Elsevier [581]

Formatted: Default Paragraph Font

Deleted: ¶ [582]

Deleted: :..., Chen, B.;..., Su, J.;..., Xu, Y.-Y.;..., Hussain, N.;..., Scaboo, K. M.;..., Zhang, Y.;..., Testa, J. M.;..., and Cai, W.-J. (2019),...: Chesapeake Bay Inorganic Carbon: Spatial Distribution and Seasonal Variability. *Front. Mar. Sci.* ... Frontiers in Marine Science, 6:99. doi: 10.3389/fmars.2019.00099 [583]

Formatted: Default Paragraph Font

Deleted: ¶ [584]

Deleted: (4417),... 409–418. [586]

Formatted [585]

Deleted: . (2004).

Deleted: .

Formatted: Default Paragraph Font, Font color: Auto, Pattern: Clear

Formatted [587]

Formatted [588]

Deleted: .

Deleted: .(2011).

Formatted [589]

Formatted [590]

Deleted: 2

Deleted: (1).

Deleted: . <https://doi.org/10.1146/annurev-marine-1>[... [593]

Formatted [591]

Formatted [592]

Formatted [594]

Deleted: ., &... and Wang, Y. (1998),...: The chem[... [595]

Deleted: (4),... 657–668. [597]

Formatted [596]

Deleted: ¶ [598]

Deleted: (8),... 1743–1752.... [600]

Formatted [599]

Formatted: Default Paragraph Font

1580 Call, M., Maher, D. T., Santos, I. R., Ruiz-Halpern, S., Mangion, P., Sanders, C. J., Erler, D. V.,
 1581 Oakes, J. M., Rosentreter, J., Murray, R., and Eyre, B. D.: Spatial and temporal variability of
 1582 carbon dioxide and methane fluxes over semi-diurnal and spring-neap-spring timescales in a
 1583 mangrove creek. *Geochimica et Cosmochimica Acta*, 150, 211–225,
 1584 <https://doi.org/10.1016/j.gca.2014.11.023>, 2015.

1585 Chen, B., Cai, W.-J., Brodeur, J. R., Hussain, N., Testa, J. M., Ni, W., and Li, Q.: Seasonal and
 1586 spatial variability in surface pCO₂ and air–water CO₂ flux in the Chesapeake Bay. *Limnology*
 1587 and *Oceanography*, 65, 3046–3065, <https://doi.org/10.1002/lno.11573>, 2020.

1588 Chen, C.-T. A., Huang, T.-H., Chen, Y.-C., Bai, Y., He, X., and Kang, Y.: Air–sea exchanges of
 1589 CO₂ in the world’s coastal seas. *Biogeosciences*, 10, 6509–6544, [https://doi.org/10.5194/bg-10-](https://doi.org/10.5194/bg-10-6509-2013)
 1590 [6509-2013](https://doi.org/10.5194/bg-10-6509-2013), 2013.

1591 Chu, S. N., Wang, Z. A., Gonnecta, M. E., Kroeger, K. D., and Ganju, N. K.: Deciphering the
 1592 dynamics of inorganic carbon export from intertidal salt marshes using high-frequency
 1593 measurements. *Marine Chemistry*, 206, 7–18, <https://doi.org/10.1016/j.marchem.2018.08.005>,
 1594 2018.

1595 Clark, J. B., Long, W., Tzortziou, M., Neale, P. J., and Hood, R. R.: Wind-Driven Dissolved
 1596 Organic Matter Dynamics in a Chesapeake Bay Tidal Marsh-Estuary System. *Estuaries and*
 1597 *Coasts*, 41, 708–723, <https://doi.org/10.1007/s12237-017-0295-1>, 2018.

1598 Clark, J. B., Long, W., and Hood, R. R.: A Comprehensive Estuarine Dissolved Organic Carbon
 1599 Budget Using an Enhanced Biogeochemical Model. *Journal of Geophysical Research:*
 1600 *Biogeosciences*, 125, e2019JG005442, <https://doi.org/10.1029/2019JG005442>, 2020.

1601 Correll, D. L., Jordan, T. E., and Weller, D. E.: Nutrient flux in a landscape: Effects of coastal
 1602 land use and terrestrial community mosaic on nutrient transport to coastal waters. *Estuaries*, 15,
 1603 431–442, <https://doi.org/10.2307/1352388>, 1992.

1604 Dai, M., Su, J., Zhao, Y., Hofmann, E. E., Cao, Z., Cai, W.-J., Gan, J., Lacroix, F., Laruelle, G.,
 1605 G., Meng, F., Müller, J. D., Regnier, P. A. G., Wang, G., and Wang, Z.: Carbon Fluxes in the
 1606 Coastal Ocean: Synthesis, Boundary Processes, and Future Trends. *Annual Review of Earth and*
 1607 *Planetary Sciences*, 50, 593–626, <https://doi.org/10.1146/annurev-earth-032320-090746>, 2022.

Deleted: JGR

Deleted: ¶

Deleted: ⋮

Deleted: ⋮

Deleted: ⋮

Deleted: ⋮

Deleted: ⋮

Deleted: ⋮

Deleted: ⋮

Formatted ... [601]

Formatted ... [602]

Formatted ... [603]

Formatted ... [604]

Formatted ... [605]

Formatted ... [606]

Formatted ... [607]

Formatted ... [608]

Deleted: ⋮

Deleted: ⋮

Deleted: ⋮

Deleted: ⋮

Deleted: Temporal Variability

Formatted ... [609]

Formatted ... [610]

Formatted ... [611]

Formatted ... [612]

Formatted ... [613]

Deleted: Carbon Dioxide

Deleted: Methane Fluxes

Deleted: Semi-Diurnal and Spring-Neap-Spring Timescales

Formatted ... [614]

Formatted ... [615]

Formatted ... [616]

Deleted: Mangrove Creek

Deleted: 2015

Deleted: <https://doi.org/10.1016/j.gca.2014.11.023>

Formatted ... [617]

Formatted ... [618]

Formatted ... [619]

Deleted: ¶

Deleted: &

Deleted: . (2020).

Formatted ... [620]

Formatted ... [621]

Formatted ... [622]

Deleted: .

Formatted ... [623]

Deleted: (12),

Deleted: <https://doi.org/10.1002/lno.11573>

Formatted ... [624]

Formatted ... [625]

Deleted: ¶

Deleted: &

Deleted: . (2013).

Formatted ... [626]

Formatted ... [627]

Formatted ... [628]

Deleted: .

Deleted: (10),

1891 [Herrmann, M., Najjar, R. G., Kemp, W. M., Alexander, R. B., Boyer, E. W., Cai, W.-J., Griffith,](#)
1892 [P. C., Kroege, K. D., McCallister, S. L., and Smith, R. A.: Net ecosystem production and](#)
1893 [organic carbon balance of U.S. East Coast estuaries: A synthesis approach, *Global*](#)
1894 [Biogeochemical Cycles](#), 29, 96–111, <https://doi.org/10.1002/2013GB004736>, 2015.

1895 [Herrmann, M., Najjar, R. G., Da, F., Friedman, J. R., Friedrichs, M. A. M., Goldberger, S.,](#)
1896 [Menendez, A., Shadwick, E. H., Stets, E. G., and St-Laurent, P.: Challenges in Quantifying Air-](#)
1897 [Water Carbon Dioxide Flux Using Estuarine Water Quality Data: Case Study for Chesapeake](#)
1898 [Bay, *Journal of Geophysical Research: Oceans*](#), 125, e2019JC015610,
1899 <https://doi.org/10.1029/2019JC015610>, 2020.

1900 [Ho, D. T., Coffineau, N., Hickman, B., Chow, N., Koffman, T., and Schlosser, P.: Influence of](#)
1901 [current velocity and wind speed on air-water gas exchange in a mangrove estuary, *Geophysical*](#)
1902 [Research Letters](#), 43, 3813–3821, <https://doi.org/10.1002/2016GL068727>, 2016.

1903 [Jiang, L.-Q., Cai, W.-J., and Wang, Y.: A comparative study of carbon dioxide degassing in](#)
1904 [river- and marine-dominated estuaries, *Limnology and Oceanography*](#), 53, 2603–2615, 2008.

1905 [Joesoef, A., Huang, W.-J., Gao, Y., and Cai, W.-J.: Air–water fluxes and sources of carbon](#)
1906 [dioxide in the Delaware Estuary: spatial and seasonal variability, *Biogeosciences*](#), 12, 6085–

1907 6101, <https://doi.org/10.5194/bg-12-6085-2015>, 2015.

1908 [Jordan, T. E. and Correll, D. L.: Continuous automated sampling of tidal exchanges of nutrients](#)
1909 [by brackish marshes, *Estuarine, Coastal and Shelf Science*](#), 32, 527–545,
1910 [https://doi.org/10.1016/0272-7714\(91\)90073-K](https://doi.org/10.1016/0272-7714(91)90073-K), 1991.

1911 [Jordan, T. E., Correll, D. L., Peterjohn, W. T., and Weller, D. E.: Nutrient flux in a landscape:](#)
1912 [The Rhode River watershed and receiving waters, in: *Watershed Research Perspectives*, edited](#)
1913 [by: Correll, D. L., Smithsonian Institution Press, Washington, DC, 1986.](#)

1914 [Jordan, T. E., Correll, D. L., Miklas, J., and Weller, D. E.: Nutrients and chlorophyll at the](#)
1915 [interface of a watershed and an estuary, *Limnol. Oceanogr.*](#), 36, 251–267,
1916 <https://doi.org/10.4319/lo.1991.36.2.0251>, 1991.

1917 [Kennedy, H., Pagès, J. F., Lagomasino, D., Arias-Ortiz, A., Colarusso, P., Fourqurean, J. W.,](#)
1918 [Githaiga, M. N., Howard, J. L., Krause-Jensen, D., Kuwae, T., Lavery, P. S., Macreadie, P. I.,](#)

- Deleted: JGR
- Moved (insertion) [4]
- Formatted ... [720]
- Deleted: &
- Deleted: . (2020).
- Formatted ... [721]
- Formatted ... [722]
- Deleted: .
- Deleted: (7),
- Deleted: .
- Formatted ... [723]
- Formatted ... [724]
- Formatted ... [725]
- Deleted: <https://doi.org/10.1029/2019JC015610>
- Formatted ... [726]
- Moved up [4]: Herrmann, M., Najjar, R. G., Kemp, W. M.,
- Deleted: et al. (2015). Net ecosystem production an ... [727]
- Formatted ... [728]
- Deleted: (8),... 3813–3821. ... [729]
- Deleted: ¶ ... [730]
- Deleted: &
- Deleted: . (2008).
- Formatted ... [731]
- Formatted ... [732]
- Formatted ... [733]
- Deleted:
- Deleted: .
- Deleted: (6),
- Deleted: . <https://doi.org/10.4319/lo.2008.53.6.2603>
- Formatted ... [734]
- Formatted ... [735]
- Formatted ... [736]
- Formatted ... [737]
- Deleted: ¶ ... [738]
- Deleted: (20),... 6085–6101. ... [740]
- Formatted ... [739]
- Deleted: ¶ ... [741]
- Deleted: (6),... 527–545. ... [743]
- Formatted ... [742]
- Moved down [5]: Jordan, T. E., Correll, D. L., Miklas, J.,
- Deleted: ¶
- Deleted: & Weller, D. E. (1991). Nutrients and chlo ... [744]
- Deleted: . Washington, DC: ... edited by: Correll, D ... [746]
- Formatted ... [745]
- Moved (insertion) [5]
- Deleted: ¶
- Deleted: -
- Formatted ... [747]
- Formatted ... [749]
- Formatted ... [750]
- Formatted ... [748]
- Deleted: -
- Deleted: . and
- Deleted: 2022. Species traits and geomorphic settin ... [753]
- Formatted ... [751]
- Formatted ... [752]

2026 [Marbà, N., Masqué, P., Mazarrasa, I., Miyajima, T., Serrano, O., and Duarte, C. M.: Species](#)
2027 [Traits and Geomorphic Setting as Drivers of Global Soil Carbon Stocks in Seagrass Meadows,](#)
2028 [Global Biogeochemical Cycles, 36, e2022GB007481, <https://doi.org/10.1029/2022GB007481>,](#)
2029 [2022.](#)

2030 [Klaus, M. and Vachon, D.: Challenges of predicting gas transfer velocity from wind](#)
2031 [measurements over global lakes, *Aquat Sci*, 82, 53, <https://doi.org/10.1007/s00027-020-00729-9>,](#)
2032 [2020.](#)

2033 [Lachin, J. M.: Fallacies of last observation carried forward analyses, *Clinical Trials*, 13, 161–](#)
2034 [168, <https://doi.org/10.1177/1740774515602688>, 2016.](#)

2035 [Laruelle, G. G., Goossens, N., Arndt, S., Cai, W.-J., and Regnier, P.: Air–water CO2 evasion](#)
2036 [from US East Coast estuaries, *Biogeosciences*, 14, 2441–2468, \[https://doi.org/10.5194/bg-14-\]\(https://doi.org/10.5194/bg-14-2441-2017\)](#)
2037 [2441-2017, 2017.](#)

2038 [Macreadie, P. I., Robertson, A. I., Spinks, B., Adams, M. P., Atchison, J. M., Bell-James, J.,](#)
2039 [Bryan, B. A., Chu, L., Filbee-Dexter, K., Drake, L., Duarte, C. M., Friess, D. A., Gonzalez, F.,](#)
2040 [Grafton, R. Q., Helmstedt, K. J., Kaebernick, M., Kelleway, J., Kendrick, G. A., Kennedy, H.,](#)
2041 [Lovelock, C. E., Megonigal, J. P., Maher, D. T., Pidgeon, E., Rogers, A. A., Sturgiss, R.,](#)
2042 [Trevathan-Tackett, S. M., Wartman, M., Wilson, K. A., and Rogers, K.: Operationalizing](#)
2043 [marketable blue carbon, *One Earth*, 5, 485–492, <https://doi.org/10.1016/j.oneear.2022.04.005>,](#)
2044 [2022.](#)

2045 [Maher, D. T. and Eyre, B. D.: Carbon budgets for three autotrophic Australian estuaries:](#)
2046 [Implications for global estimates of the coastal air–water CO2 flux, *Global Biogeochemical*](#)
2047 [Cycles, 26, <https://doi.org/10.1029/2011GB004075>, 2012.](#)

2048 [Martin, C. R., Zeng, N., Karion, A., Dickerson, R. R., Ren, X., Turpie, B. N., and Weber, K. J.:](#)
2049 [Evaluation and environmental correction of ambient CO2 measurements from a low-cost NDIR](#)
2050 [sensor, *Atmospheric Measurement Techniques*, 10, 2383–2395, \[https://doi.org/10.5194/amt-10-\]\(https://doi.org/10.5194/amt-10-2383-2017\)](#)
2051 [2383-2017, 2017.](#)

2052 [Menendez, A., Tzortziou, M., Neale, P., Megonigal, P., Powers, L., Schmitt-Kopplin, P., and](#)
2053 [Gonsior, M.: Strong Dynamics in Tidal Marsh DOC Export in Response to Natural Cycles and](#)

Deleted: JGR
Formatted (... [754])
Deleted: (10) p.
Formatted (... [755])
Deleted: :
Formatted (... [756])
Deleted: ., &... and Vachon, D. (2020).....: Challeng (... [757])
Formatted (... [758])
Deleted: (3),... 53. (... [759])
Deleted: ¶ (... [760])
Formatted (... [761])
Deleted: (2),... 161–168. (... [762])
Deleted: ¶ (... [763])
Formatted (... [764])
Deleted: &
Formatted (... [764])
Deleted: . (2017).
Formatted (... [765])
Deleted: .
Formatted (... [766])
Deleted: (9),
Formatted (... [767])
Deleted: .
Deleted: <https://doi.org/10.5194/bg-14-2441-2017>
Formatted (... [768])
Formatted (... [769])
Deleted: ¶ (... [770])
Formatted (... [770])
Deleted: . and Duarte, C.M., 2022.
Formatted (... [771])
Deleted: .
Deleted: (5):
Deleted: -
Formatted (... [772])
Formatted (... [773])
Formatted (... [774])
Deleted: ¶ (... [775])
Deleted: .,
Deleted:
Deleted: . (2012),
Formatted (... [775])
Formatted (... [776])
Formatted (... [777])
Formatted (... [778])
Deleted: flux, *Global Biogeochem. Cycles*, 26, GB (... [779])
Formatted (... [780])
Deleted: ¶ (... [781])
Deleted: (7),... 2383–2395. (... [783])
Formatted (... [782])
Deleted: ¶ (... [784])

2126 Episodic Events From Continuous Monitoring, *Journal of Geophysical Research:*
2127 *Biogeosciences*, 127, e2022JG006863, <https://doi.org/10.1029/2022JG006863>, 2022.

2128 Miller, A. W., Reynolds, A. C., and Minton, M. S.: A spherical falling film gas-liquid
2129 equilibrator for rapid and continuous measurements of CO₂ and other trace gases, *PLOS ONE*,
2130 14, e0222303, <https://doi.org/10.1371/journal.pone.0222303>, 2019.

2131 Najjar, R. G., Herrmann, M., Cintrón Del Valle, S. M., Friedman, J. R., Friedrichs, M. A. M.,
2132 Harris, L. A., Shadwick, E. H., Stets, E. G., and Woodland, R. J.: Alkalinity in Tidal Tributaries
2133 of the Chesapeake Bay, *Journal of Geophysical Research: Oceans*, 125, e2019JC015597,
2134 <https://doi.org/10.1029/2019JC015597>, 2020.

2135 Oreska, M. P. J., McGlathery, K. J., Aoki, L. R., Berger, A. C., Berg, P., and Mullins, L.: The
2136 greenhouse gas offset potential from seagrass restoration, *Sci Rep*, 10, 7325,
2137 <https://doi.org/10.1038/s41598-020-64094-1>, 2020.

2138 Raymond, P. A. and Cole, J. J.: Gas Exchange in Rivers and Estuaries: Choosing a Gas Transfer
2139 Velocity, *Estuaries*, 24, 312–317, <https://doi.org/10.2307/1352954>, 2001.

2140 Raymond, P. A., Hartmann, J., Lauerwald, R., Sobek, S., McDonald, C., Hoover, M., Butman,
2141 D., Striegl, R., Mayorga, E., Humborg, C., Kortelainen, P., Dürr, H., Meybeck, M., Ciais, P., and
2142 Guth, P.: Global carbon dioxide emissions from inland waters, *Nature*, 503, 355–359,
2143 <https://doi.org/10.1038/nature12760>, 2013.

2144 Rose, K. C., Neale, P. J., Tzortziou, M., Gallegos, C. L., and Jordan, T. E.: Patterns of spectral,
2145 spatial, and long-term variability in light attenuation in an optically complex sub-estuary,
2146 *Limnology and Oceanography*, 64, S257–S272, <https://doi.org/10.1002/lno.11005>, 2019.

2147 Rosentreter, J. A., Wells, N. S., Ulseth, A. J., and Eyre, B. D.: Divergent Gas Transfer Velocities
2148 of CO₂, CH₄, and N₂O Over Spatial and Temporal Gradients in a Subtropical Estuary, *Journal*
2149 *of Geophysical Research: Biogeosciences*, 126, e2021JG006270,
2150 <https://doi.org/10.1029/2021JG006270>, 2021.

2151 Saba, G. K., Goldsmith, K. A., Cooley, S. R., Grosse, D., Meseck, S. L., Miller, A. W., Phelan,
2152 B., Poach, M., Rheault, R., St-Laurent, K., Testa, J. M., Weis, J. S., and Zimmerman, R.:
2153 Recommended priorities for research on ecological impacts of ocean and coastal acidification in

Deleted: JGR
Deleted: .
Formatted ... [785]
Deleted: (7),... e2022JG006863. ... [786]
Deleted: ¶ ... [787]
Formatted ... [788]
Deleted: (9),... e0222303. ... [789]
Deleted: ¶ ... [790]
Formatted ... [791]
Deleted: ¶ ... [792]
Deleted: (1), ... [793]
Formatted ... [794]
Deleted: ¶ ... [795]
Deleted: ., & ... [796]
Deleted: . (2001). ... [797]
Formatted ... [798]
Formatted ... [799]
Formatted ... [800]
Formatted ... [801]
Formatted ... [802]
Deleted: ¶ ... [803]
Deleted: & ... [804]
Deleted: . (2013). ... [805]
Deleted: (7476), Article 7476. ... [806]
Formatted ... [807]
Formatted ... [808]
Deleted: https://doi.org/10.1038/nature12760 ... [809]
Formatted ... [810]
Deleted: (S1),... S257–S272. ... [811]
Formatted ... [812]
Deleted: ¶ ... [813]
Formatted ... [814]
Deleted: (10),... e2021JG006270. ... [815]
Deleted: ¶ ... [816]
Deleted: et al. (2019). ... [817]
Formatted ... [818]

2223 the *U.S. Mid-Atlantic, Estuarine, Coastal and Shelf Science*, 225, 106188,
2224 <https://doi.org/10.1016/j.ecss.2019.04.022>, 2019.

2225 Saucier, W. J.: Principles of Meteorological Analysis, Dover Publications, 468 pp., 2003.

2226 Song, S., Wang, Z. A., Kroeger, K. D., Eagle, M., Chu, S. N., and Ge, J.: High-frequency
2227 variability of carbon dioxide fluxes in tidal water over a temperate salt marsh, *Limnology and*
2228 *Oceanography*, 68, 2108–2125, <https://doi.org/10.1002/lno.12409>, 2023.

2229 Spada, S., Quartagno, M., Tamburini, M., and Robinson, D.: orcutt: Estimate Procedure in Case
2230 of First Order Autocorrelation, 2018.

2231 Sun, X., Alcalde, J., Bakhtbidar, M., Elío, J., Vilarrasa, V., Canal, J., Ballesteros, J., Heinemann,
2232 N., Haszeldine, S., Cavanagh, A., Vega-Maza, D., Rubiera, F., Martínez-Orio, R., Johnson, G.,
2233 Carbonell, R., Marzan, I., Travé, A., and Gomez-Rivas, E.: Hubs and clusters approach to unlock
2234 the development of carbon capture and storage – Case study in Spain, *Applied Energy*, 300,
2235 117418, <https://doi.org/10.1016/j.apenergy.2021.117418>, 2021.

2236 *Susquehanna River at Conowingo, MD | U.S. Geological Survey:*
2237 <https://waterdata.usgs.gov/monitoring-location/01578310/>, last access: 28 September 2023.

2238 Takahashi, T., Sutherland, S. C., Sweeney, C., Poisson, A., Metzl, N., Tilbrook, B., Bates, N.,
2239 Wanninkhof, R., Feely, R. A., Sabine, C., Olafsson, J., and Nojiri, Y.: Global sea–air CO₂ flux
2240 based on climatological surface ocean pCO₂, and seasonal biological and temperature effects,
2241 *Deep Sea Research Part II: Topical Studies in Oceanography*, 49, 1601–1622.
2242 [https://doi.org/10.1016/S0967-0645\(02\)00003-6](https://doi.org/10.1016/S0967-0645(02)00003-6), 2002.

2243 Thoning, K. W., Crotwell, A. M., and Mund, J. W.: NOAA Global Monitoring Laboratory
2244 Carbon Cycle and Greenhouse Gases Group Continuous *In situ* Measurements of CO₂ at Global
2245 Background Sites, 1973–Present, <https://doi.org/10.15138/YAF1-BK21>, 2023.

2246 Tzortziou, M., Neale, P. J., Osburn, C. L., Megonigal, J. P., Maie, N., and Jaffé, R.: Tidal
2247 marshes as a source of optically and chemically distinctive colored dissolved organic matter in
2248 the Chesapeake Bay, *Limnology and Oceanography*, 53, 148–159.
2249 <https://doi.org/10.4319/lo.2008.53.1.0148>, 2008.

- Deleted: JGR
- Deleted: US...S. Mid-Atlantic. (... [817])
- Deleted: :
- Formatted (... [818])
- Deleted: ¶
- Deleted: (2003).
- Deleted: .
- Deleted: New York
- Formatted (... [819])
- Formatted (... [820])
- Formatted (... [821])
- Formatted (... [822])
- Deleted: ↵
- Deleted: &
- Deleted: (2023).
- Formatted (... [823])
- Formatted (... [824])
- Formatted (... [825])
- Deleted: .
- Formatted (... [826])
- Deleted: .
- Formatted (... [827])
- Deleted: ↵ (... [828])
- Formatted (... [829])
- Deleted: ↵ (... [830])
- Formatted (... [831])
- Deleted: ... <https://doi.org/10.1016/j.apenergy.2021.117418> (... [832])
- Deleted: et al. (2002).
- Formatted (... [833])
- Deleted: .
- Formatted (... [834])
- Deleted: (9),... 1601–1622. (... [836])
- Formatted (... [835])
- Formatted (... [837])
- Deleted: ¶ (... [838])
- Formatted (... [839])
- Moved down [6]: Tzortziou, M., Neale, P. J., Megonigal, J.
- Deleted: ¶
- Deleted: & Butterworth, M. (2011). Spatial gradient (... [840])
- Deleted: (1),... 148–159. (... [842])
- Formatted (... [841])
- Formatted (... [843])

2325 [Tzortziou, M., Neale, P. J., Megonigal, J. P., Pow, C. L., and Butterworth, M.: Spatial gradients](#)
2326 [in dissolved carbon due to tidal marsh outwelling into a Chesapeake Bay estuary, *Marine*](#)
2327 [Ecology Progress Series](#), 426, 41–56, <https://doi.org/10.3354/meps09017>, 2011.

2328 [Unsworth, R. K. F., Cullen-Unsworth, L. C., Jones, B. L. H., and Lilley, R. J.: The planetary role](#)
2329 [of seagrass conservation, *Science*](#), 377, 609–613, <https://doi.org/10.1126/science.abq6923>, 2022.

2330 [Upstill-Goddard, R. C.: Air–sea gas exchange in the coastal zone, *Estuarine, Coastal and Shelf*](#)
2331 [Science](#), 70, 388–404, <https://doi.org/10.1016/j.ecss.2006.05.043>, 2006.

2332 [Van Dam, B. R., Edson, J. B., and Tobias, C.: Parameterizing Air–Water Gas Exchange in the](#)
2333 [Shallow, Microtidal New River Estuary, *Journal of Geophysical Research: Biogeosciences*](#), 124,
2334 2351–2363, <https://doi.org/10.1029/2018JG004908>, 2019.

2335 [Wanninkhof, R.: Relationship between wind speed and gas exchange over the ocean, *Journal of*](#)
2336 [Geophysical Research: Oceans](#), 97, 7373–7382, 1992.

2337 [Wanninkhof, R.: Relationship between wind speed and gas exchange over the ocean revisited,](#)
2338 [Limnology and Oceanography: Methods](#), 12, 351–362, <https://doi.org/10.4319/lom.2014.12.351>,

2339 2014.

2340 [Wanninkhof, R. and McGillis, W. R.: A cubic relationship between air–sea CO2 exchange and](#)
2341 [wind speed, *Geophysical Research Letters*](#), 26, 1889–1892,

2342 <https://doi.org/10.1029/1999GL900363>, 1999.

2343 [Wanninkhof, R., Park, G.-H., Takahashi, T., Sweeney, C., Feely, R., Nojiri, Y., Gruber, N.,](#)
2344 [Doney, S. C., McKinley, G. A., Lenton, A., Le Quéré, C., Heinze, C., Schwinger, J., Graven, H.,](#)
2345 [and Khatiwala, S.: Global ocean carbon uptake: magnitude, variability and trends,](#)
2346 [Biogeosciences](#), 10, 1983–2000, <https://doi.org/10.5194/bg-10-1983-2013>, 2013.

2347 [Waycott, M., Duarte, C. M., Carruthers, T. J. B., Orth, R. J., Dennison, W. C., Olyarnik, S.,](#)
2348 [Calladine, A., Fourqurean, J. W., Heck, K. L., Hughes, A. R., Kendrick, G. A., Kenworthy, W.](#)
2349 [J., Short, F. T., and Williams, S. L.: Accelerating loss of seagrasses across the globe threatens](#)
2350 [coastal ecosystems, *Proceedings of the National Academy of Sciences*](#), 106, 12377–12381,

2351 <https://doi.org/10.1073/pnas.0905620106>, 2009.

Deleted: JGR

Moved (insertion) [6]

Deleted: ¶

Deleted: , 2022.

Formatted ... [844]

Formatted ... [846]

Formatted ... [847]

Formatted ... [845]

Deleted: ,

Deleted: (6606), pp.609-613

Formatted ... [848]

Formatted ... [849]

Deleted: ¶

Deleted: (2006),...: Air–sea gas exchange in the co... [851]

Formatted ... [852]

Formatted ... [850]

Deleted: (3),... 388–404. [853]

Formatted ... [854]

Deleted: |U.S. Geological Survey (2023). Freshwater... [855]

Deleted: (7),... 2351–2363. [857]

Formatted ... [856]

Deleted: ¶ [858]

Formatted ... [859]

Deleted: (C5),

Deleted: ¶ [860]

Deleted: (6),... 351–362. [862]

Formatted ... [861]

Deleted: ¶ [863]

Deleted: (13),... 1889–1892. [865]

Formatted ... [864]

Deleted: et al. (2013)...ruber, N., Doney, S. C., Mc... [866]

Deleted: (3),... 1983–2000. [868]

Formatted ... [867]

Formatted ... [869]

Deleted: ¶

Deleted: +10, and Susan L.

Formatted ... [870]

Deleted: (2009).

Formatted ... [871]

Formatted ... [872]

Deleted: ,

Deleted: (30):

Deleted: ¶

Formatted ... [873]

Formatted ... [874]

Formatted ... [875]

Formatted ... [876]

2442 Weiss, R. and Price, B.: Nitrous oxide solubility in water and seawater, *Marine Chemistry*, 8,
2443 347–359, [https://doi.org/10.1016/0304-4203\(80\)90024-9](https://doi.org/10.1016/0304-4203(80)90024-9), 1980.

2444 Winslow, L. A., Zwart, J. A., Batt, R. D., Dugan, H. A., Woolway, R. I., Corman, J. R., and
2445 Read, J. S.: LakeMetabolizer: An R package for estimating lake metabolism from free-water
2446 oxygen using diverse statistical models, *Inland Waters*, 6, <https://doi.org/10.1080/IW-6.4.883>,
2447 2016.

2448 Xiao, S., Liu, L., Wang, W., Lorke, A., Woodhouse, J., and Grossart, H.-P.: A Fast-Response
2449 Automated Gas Equilibrator (FaRAGE) for continuous *in situ* measurement of CH₄ and CO₂
2450 dissolved in water, *Hydrology and Earth System Sciences*, 24, 3871–3880.
2451 <https://doi.org/10.5194/hess-24-3871-2020>, 2020.

2452 Zeebe, R. E. and Wolf-Gladrow, D.: CO₂ in Seawater: Equilibrium, Kinetics, Isotopes, Gulf
2453 Professional Publishing, 382 pp., 2001.

2454

Deleted: JGR

Deleted: , &... and Price, B. (1980)...: Nitrous oxide solubility in water and seawater. ... [877]

Deleted: (4),... 347–359. ... [879]

Formatted ... [878]

Formatted: Default Paragraph Font

Deleted: ¶ ... [880]

Deleted: : *Journal of the International Society of Limnology*

Deleted: (4).

Formatted: Font: Not Italic

Formatted: Font: Not Italic

Formatted: Default Paragraph Font

Deleted: ¶

Deleted: ¶

Deleted: ¶

Deleted: ¶

Formatted: Default Paragraph Font

Formatted: Default Paragraph Font

Formatted: Default Paragraph Font

Formatted: Default Paragraph Font

Deleted: ¶

Deleted: ¶

Formatted: Default Paragraph Font

Formatted: Default Paragraph Font

Deleted: C

Deleted: [Situ Measurement](#)

Formatted: Default Paragraph Font

Formatted ... [881]

Deleted: D

Deleted: [Water \(2020\)](#).

Deleted: (7).

Deleted: : <https://doi.org/10.5194/hess-24-3871->

Formatted: Default Paragraph Font

Formatted ... [882]

Formatted: Default Paragraph Font

Formatted: Default Paragraph Font

Deleted: ¶ ... [883]

Deleted: .

Formatted: Font: Not Italic

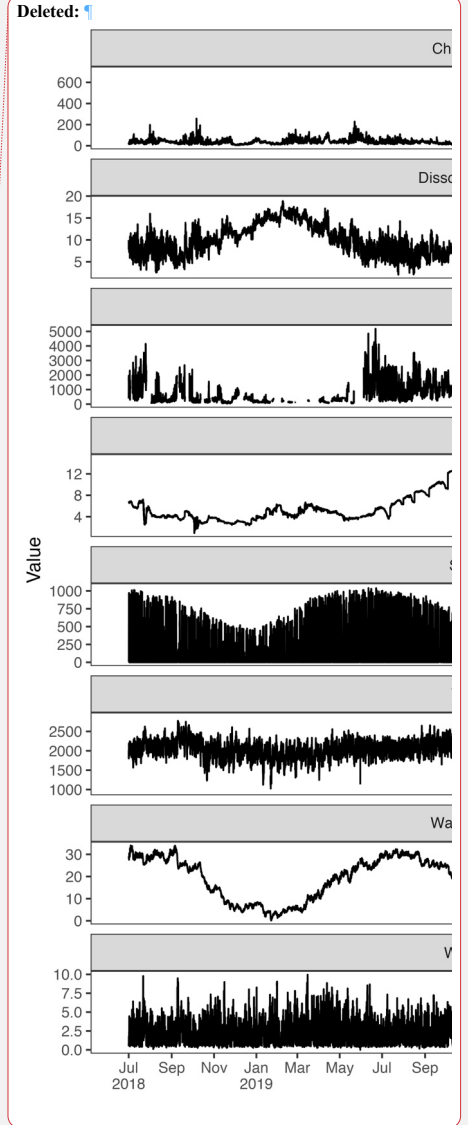
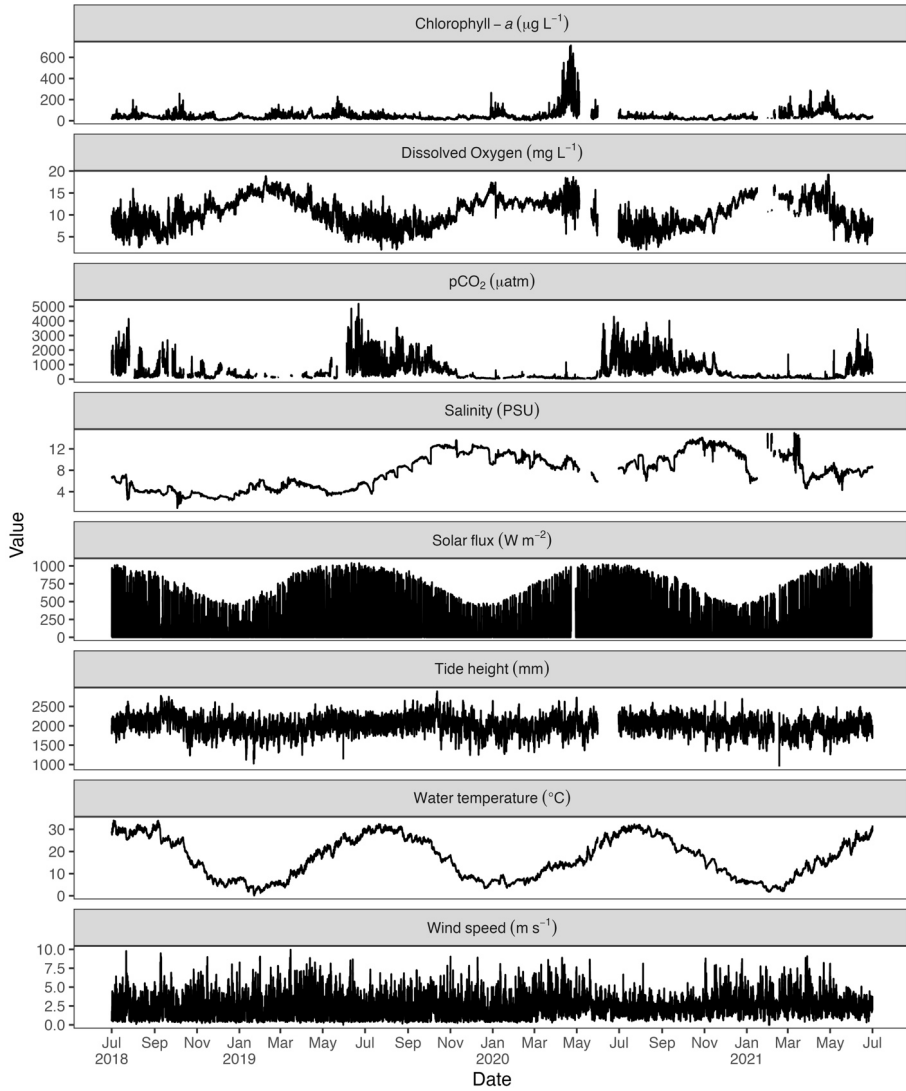
Deleted: ¶

¶

¶ ... [884]

Deleted: JGR

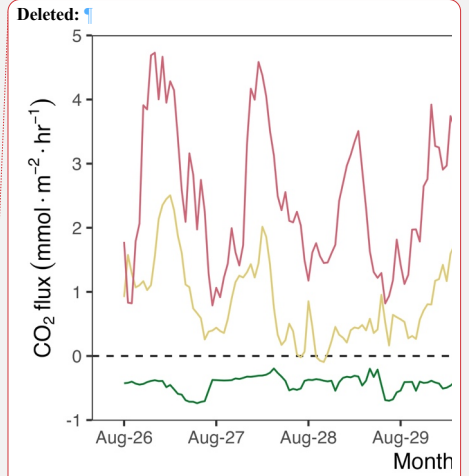
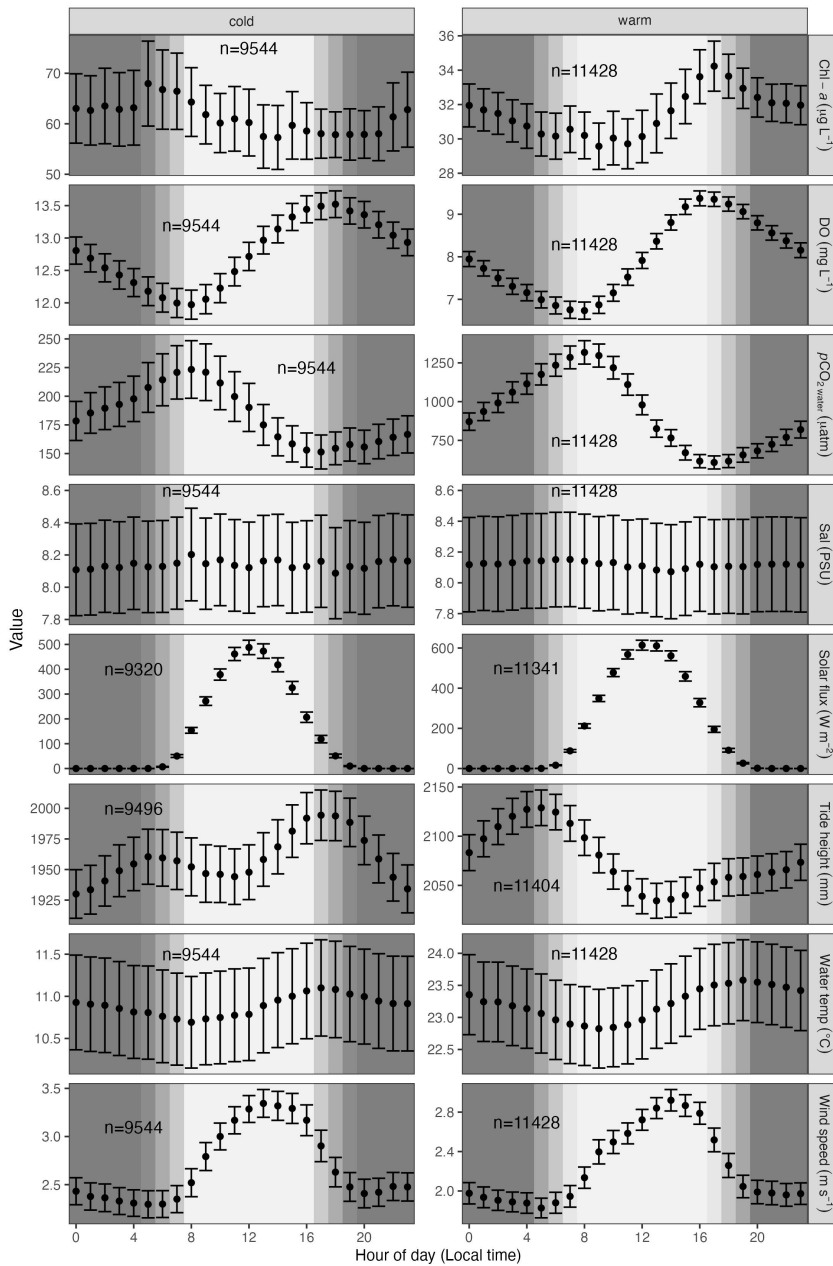
2533 Supplemental



2534
2535
2536

Fig. S1. Plot of all raw values from environmental variables for the same time period as CO₂ flux (July 2018–July 2021).

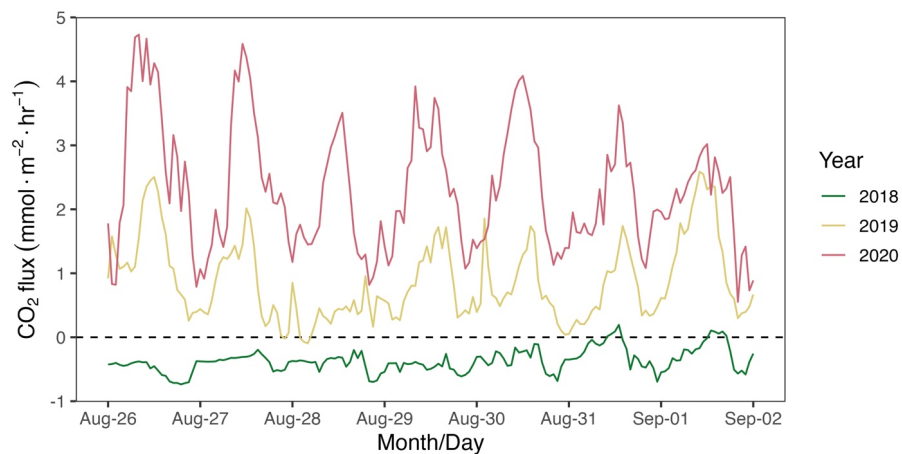
Deleted: JGR



Deleted: JGR

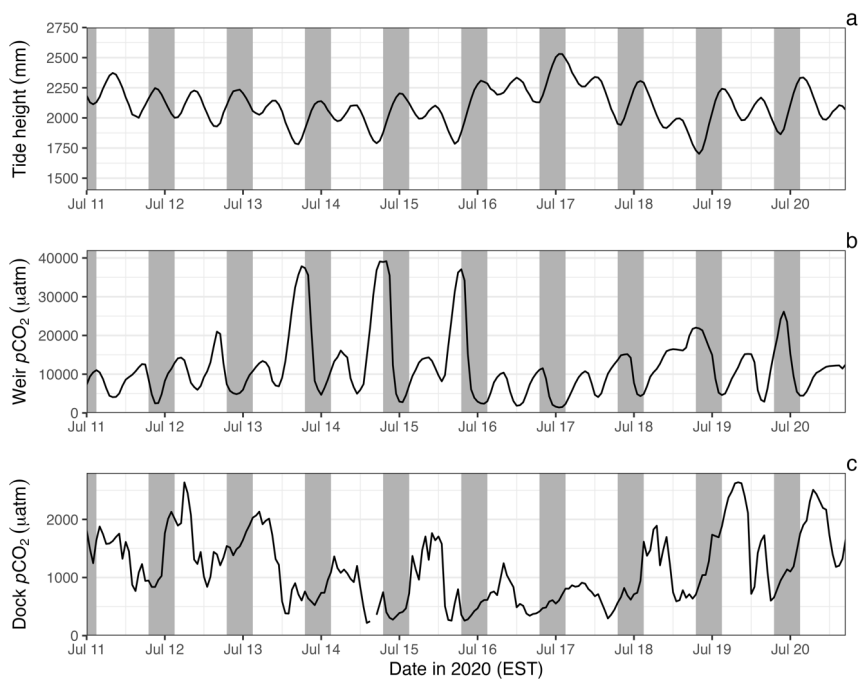
2542 **Fig. S2.** Average hourly values (95% CI) of environmental variables across 24 hours of the day
2543 (July 2018–July 2021) in cold and warm seasons. Light/dark background indicates day/night
2544 conditions.
2545
2546

Formatted: Font: Not Bold



2547 **Fig. S3.** Hourly CO₂ flux estimates for the week of August 26 to September 2 where CO₂ flux
2548 status differs among years.
2549
2550

Deleted: JGR



2551
 2552 **Fig. S4.** Simultaneous $p\text{CO}_2$ measurements (1 hr intervals) from SERC dock (panel c) and the
 2553 mouth of the single tidal creek that drains the Kirkpatrick Marsh (panel b) (11–20 Jul 2020)
 2554 indicate that dissolved CO_2 varies at the dock according to a day/night cycle while CO_2 in the
 2555 marsh tidal creek rises and falls inversely with tide height (panel a), indicating outwelling of
 2556 marsh derived CO_2 (e.g., root respiration, pore and groundwater).

Deleted: S3

Deleted: -

Deleted: -